OPEN ACCESS Freely available online

PLoS GENETICS

Arabidopsis COMPASS-Like Complexes Mediate Histone H3 Lysine-4 Trimethylation to Control Floral Transition and Plant Development

Danhua Jiang[1,2], Nicholas C. Kong[1,2], Xiaofeng Gu[2], Zicong Li[1], Yuehui He[1,2]*

1 Department of Biological Sciences, National University of Singapore, Singapore, Singapore, **2** Temasek Life Sciences Laboratory, Singapore, Singapore

Abstract

Histone H3 lysine-4 (H3K4) methylation is associated with transcribed genes in eukaryotes. In *Drosophila* and mammals, both di- and tri-methylation of H3K4 are associated with gene activation. In contrast to animals, in *Arabidopsis* H3K4 trimethylation, but not mono- or di-methylation of H3K4, has been implicated in transcriptional activation. H3K4 methylation is catalyzed by the H3K4 methyltransferase complexes known as COMPASS or COMPASS-like in yeast and mammals. Here, we report that *Arabidopsis* homologs of the COMPASS and COMPASS-like complex core components known as Ash2, RbBP5, and WDR5 in humans form a nuclear subcomplex during vegetative and reproductive development, which can associate with multiple putative H3K4 methyltransferases. Loss of function of *ARABIDOPSIS* Ash2 RELATIVE (ASH2R) causes a great decrease in genome-wide H3K4 trimethylation, but not in di- or mono-methylation. Knockdown of *ASH2R* or the *RbBP5* homolog suppresses the expression of a crucial *Arabidopsis* floral repressor, *FLOWERING LOCUS C* (*FLC*), and *FLC* homologs resulting in accelerated floral transition. ASH2R binds to the chromatin of *FLC* and *FLC* homologs *in vivo* and is required for H3K4 trimethylation, but not for H3K4 dimethylation in these loci; overexpression of *ASH2R* causes elevated H3K4 trimethylation, but not H3K4 dimethylation, in its target genes *FLC* and *FLC* homologs, resulting in activation of these gene expression and consequent late flowering. These results strongly suggest that H3K4 trimethylation in *FLC* and its homologs can activate their expression, providing concrete evidence that H3K4 trimethylation accumulation can activate eukaryotic gene expression. Furthermore, our findings suggest that there are multiple COMPASS-like complexes in *Arabidopsis* and that these complexes deposit trimethyl but not di- or mono-methyl H3K4 in target genes to promote their expression, providing a molecular explanation for the observed coupling of H3K4 trimethylation (but not H3K4 dimethylation) with active gene expression in *Arabidopsis*.

Citation: Jiang D, Kong NC, Gu X, Li Z, He Y (2011) *Arabidopsis* COMPASS-Like Complexes Mediate Histone H3 Lysine-4 Trimethylation to Control Floral Transition and Plant Development. PLoS Genet 7(3): e1001330. doi:10.1371/journal.pgen.1001330

Editor: Gregory P. Copenhaver, The University of North Carolina at Chapel Hill, United States of America

Received June 23, 2010; **Accepted** February 8, 2011; **Published** March 10, 2011

Funding: This work was supported by the Singapore Ministry of Education (AcRF Tier 2; MOE2009-T2-1-081) and by the Temasek Life Sciences Laboratory to YH. The funders had no role in study design, data collection and analysis, decision to publish, or preparation of the manuscript.

Competing Interests: The authors have declared that no competing interests exist.

* E-mail: dbshy@nus.edu.sg

Introduction

Histone lysine methylation regulates chromatin structure and gene transcription in eukaryotes. Various lysine residues on histones can be methylated and the ε-amino group of lysines can be mono-, di- and tri-methylated. Lysine methylation is linked with transcriptional activation or repression depending on the particular residue that is methylated and the degree of methylation [1]. For instance, H3 lysine-27 trimethylation (H3K27me3) is exclusively involved in transcriptional repression, whereas H3K4 trimehtylation is associated with actively transcribed genes [2].

Recent genome-scale analyses of H3K4 methylation have revealed that different H3K4 methylation states are often associated with distinct transcription states in a gene. In the well-studied *Saccharomyces cerevisiae*, H3K4 trimethylation is a mark for actively transcribed genes, whereas mono- or di-methylation of H3K4 is not linked with active gene expression [3]. In *Drosophila* and mammals, both di- and tri-methylation of H3K4 are associated with gene activation [4,5]. In contrast to animals, in the higher plant *Arabidopsis thaliana*, only H3K4 trimethylation, but not mono- or di-methylation of H3K4, is implicated in transcriptional activation [6].

H3K4 methylation is catalyzed by various methyltransferases. In *Saccharomyces cerevisiae*, the COMPASS (for Complex Proteins Associated with Set1) H3K4 methyltransferase complex catalyzes H3K4 methylation [7]. This complex contains an H3K4 methyltransferase called Set1, the only known H3K4 methyltransferase in yeast. By itself, Set1 is unable to catalyze H3K4 methylation, and requires other structural components in the complex for its catalytic activity [8,9]. COMPASS-like complexes have been identified in mammals, and so far, five such complexes known as hSet1 and MLL1, MLL2, MLL3 and MLL4 have been biochemically purified [for a review, see [2]]. All of these complexes contain four core components including an H3K4 methyltransferase and three structural core components known as WDR5, Ash2 and RbBP5, homologs of the yeast SWD3, BRE2 and SWD1, respectively [2]. WDR5, Ash2 and RbBP5 together form a stable core subcomplex that provides a structural platform for H3K4 methylation [10]. The Ash2-RbBP5-WDR5 subcomplex interchangeably associates with different H3K4 methyltransferases such as hSet1, MLL1 and MLL2 to form different catalytic

Author Summary

Histones can be covalently modified and histone modifications regulate chromatin structure and gene transcription. One such modification is histone H3 lysine-4 (H3K4) methylation, which can be mono-, di-, or tri-methylated. In animals such as fruitfly and mammals, both di- and tri-methylation of H3K4 are associated with active gene expression. In contrast to animals, in the flowering plant *Arabidopsis* only H3K4 trimethylation has been implicated in gene transcriptional activation. H3K4 methylation is catalyzed by the H3K4 methyltransferase complexes known as COMPASS-like in mammals. Here, we report that COMPASS-like H3K4 methyltransferase complexes exist in *Arabidopsis*. Loss of function of a core complex protein causes a great decrease in *Arabidopsis* genome-wide H3K4 trimethylation, but not in di- or mono-methylation. Our analyses of several direct target genes of these COMPASS-like complexes show that they mediate deposition of trimethyl but not dimethyl H3K4 in these loci to activate their expression, providing concrete evidence for the notion that H3K4 trimethylation accumulation can activate eukaryotic gene expression. Furthermore, our findings provide a molecular explanation for the observed coupling of trimethylation but not dimethylation of H3K4 with active gene expression in *Arabidopsis*. In addition, we found that H3K4 trimethylation regulates leaf growth and development, flowering, and embryo development.

complexes, and is essential for both di- and tri-methylation of H3K4 [9,10]. An *in vitro* reconstituted four-component mini-complex composed of WDR5, Ash2, RbBP5 and MLL1 methylates H3K4 specifically [9]. So far, COMPASS-like complexes have been identified in mammals, but still remain to be identified in other multicellular organisms such as plants.

H3K4 trimethylation typically occurs concomitantly with active gene transcription, and trimethyl H3K4 (H3K4me3) predominantly accumulates in the 5′ transcribed regions [2,11]. In yeast, the RNA Polymerase II Associated Factor 1 complex (Paf1c) recruits the COMPASS complex to the initiating and early-elongating RNA Polymerase II (Pol II), resulting in H3K4 trimethylation in the 5′ genic regions [12]. A similar mechanism might exist in multicellular organisms as Paf1c appears to be evolutionarily conserved in animals and plants [13–15]. Although H3K4me3 is a chromatin mark for actively transcribed genes, whether it plays an active role in transcriptional activation remains unclear because the accumulation of H3K4me3 in the 5′ transcribed regions might merely result from active transcription by Pol II [16].

Recent studies have revealed a few components involved in H3K4 methylation in *Arabidopsis*. It has been shown that the *Arabidopsis* Paf1c is required for the accumulation of H3K4me3 in the 5′ regions of actively transcribed genes in *Arabidopsis* genome [15]. Bioinformatic and phylogenetic analyses reveal that there may be up to ten putative *Arabidopsis* H3K4 methyltransferases, among which are *ARABIDOPSIS* TRITHORAX1 (ATX1), ATX2, SET DOMAIN PROTEIN25 (SDG25; also known as ATXR7), SDG14 and SDG16 [17,18]. Loss of *ATX1* function causes a slight reduction in global H3K4me3 and accelerated developmental transition from a vegetative to a reproductive phase (*i.e.*, flowering) [19]. In addition, *atx1* mutation leads to floral organ abnormalities in a particular *Arabidopsis* ecotype [20]. Recently, it has been shown that loss of *ATX2* or *ATXR7* function causes moderately early flowering [21–23]. Besides these putative H3K4 methyltransferases, *Arabidopsis* has two homologs of the human COMPASS-like complex core component WDR5, namely WDR5a and WDR5b [24]. WDR5a binds histone H3 tails, is involved in H3K4 methylation in its target gene chromatin, and represses *Arabidopsis* flowering [24].

The timing of floral transition in *Arabidopsis* is genetically controlled by a network of flowering genes, among which *FLC* plays a central role. FLC, a MADS box transcriptional factor, is a key floral repressor that quantitatively inhibits the floral transition in *Arabidopsis* [for a review, see [25,26]]. Besides *FLC*, there are five *FLC* homologs in *Arabidopsis*: *FLOWERING LOCUS M* (*FLM*)/*MADS BOX AFFECTING FLOWERING 1* (*MAF1*) and *MAF2*-*MAF5* [27,28]. *FLM*, *MAF2* and *MAF4* moderately repress flowering [27–29], whereas the roles for *MAF3* and *MAF5* remain unclear [28].

FLC expression is under complex control and chromatin modification plays a critical role in *FLC* regulation which has become a model for understanding plant gene regulation by chromatin-based mechanisms [26,30,31]. *FLC* is expressed at low levels in many early-flowering *Arabidopsis* accessions because of the repression by 'autonomous-pathway' genes, among which are a few histone modifiers including CURLY LEAF (a putative H3K27 methyltransferase), HISTONE DEACETYLASE6, FLOWERING LOCUS D (FLD, a putative H3K4 demethylase) and several Type I and II arginine methyltransferases [32–36]. These proteins mediate 'repressive' histone modifications in *FLC* chromatin and repress *FLC* expression to promote flowering. In addition to repressive histone modifications, *FLC* chromatin can also be modified by H3K4 methylation. Recent studies have revealed that H3K4 trimethylation is linked with activation of *FLC* expression. H3K4me3 accumulates in the region around the transcription start site (TSS) of *FLC* including the 5′ end of transcribed region [13,21]. This modification requires Paf1c and WDR5a, and in addition, ATX1 and ATXR7 are partly required [13,15,21,22,24,37]. WDR5a can interact with ATX1, binds to *FLC* chromatin, is required for H3K4 trimethylation in *FLC* and for *FLC* activation, and has been proposed to act in the context of an H3K4 methyltransferase complex [24]. So far, although several components involved in H3K4 methylation have been characterized in *Arabidopsis*, it remains essentially unknown whether H3K4 methyltransferase complexes exist in *Arabidopsis*. In addition, although it has been well documented that H3K4me3 accumulation is associated with actively transcribed *FLC* chromatin, whether H3K4 trimethylation can activate *FLC* expression is unknown.

Here, we report that *Arabidopsis* homologs of the human COMPASS-like complex core components Ash2 and RbBP5, together with WDR5a, form a nuclear subcomplex for H3K4 methylation during vegetative and reproductive development. The subcomplex component WDR5a can associate with several putative H3K4 methyltransferases, suggesting that multiple COMPASS-like complexes exist in *Arabidopsis*. Loss of *ASH2R* function causes a great decrease in genome-wide H3K4 trimethylation, but not di- or mono-methylation. In addition, we found that the ASH2R subcomplex mediates H3K4 trimethylaiton, but not H3K4 dimethylation, in *FLC* and *FLC* homologs to activate their expression resulting in delayed flowering. Our findings suggest that the ASH2R-containing COMPASS-like complexes (ASH2R-COMPASS) deposit H3K4me3, but not H3K4me2 or H3K4me1 in *Arabidopsis* genome. Furthermore, we found that a null lesion in *ASH2R* causes arrested embryo development at globular stage and that *ASH2R* is also required for proper leaf growth and development, suggesting that the ASH2R-COMPASS-mediated H3K4 trimethylation plays important roles for multiple *Arabidopsis* developmental processes.

Results

Identification and Phylogenetic Analyses of *Arabidopsis* Homologs of the Human COMPASS-Like Complex Core Components, Ash2, RbBP5, and WDR5

Recently we have identified two homologs of the human WDR5, namely WDR5a and WDR5b in *Arabidopsis* genome [24]. To explore whether homologs of the other core COMPASS-like complex components Ash2 and RbBP5, exist in *Arabidopsis*, we searched the *Arabidopsis* protein database with the amino acid sequences of these proteins and identified a single homolog for each protein, namely ASH2R (At_1g51450) and RbBP5 LIKE (RBL; At_3g21060) (Figure S1 and Figure S2). The sequence similarity between ASH2R and the human Ash2 over the entire ASH2R is 46% (Figure S1). A recent phylogenetic analysis of Ash2 homologs from several animals and plants also indicates that ASH2R (also known as TRO) is a clear homolog of the human Ash2 [38]. We carried out phylogenetic analysis of RbBP5 homologs from representative animal and plant species. As shown in Figure S2, in each animal or plant species examined, there is only a single RbBP5 homolog; animal RbBP5 homologs form one clade, and plant homologs constitute another clade. These findings show that there are Ash2 and RbBP5 homologs in *Arabidopsis*.

The evolutionary history of WDR5 homologs is complex. We found that there are multiple WDR5 homologs in land plants, for instance, three in the basal land plant moss, two in the monocot rice and three in the eudicot poplar, whereas in most animals, there is only a single WDR5 homolog (Figure 1). We further performed phylogenetic analysis of WDR5 homologs from representative species. The phylogenetic tree indicates that all WDR5 homologs from plants form a single clade with 64 bootstrap support, whereas all animal WDR5 homologs form another clade with 67 bootstrap support (Figure 1). There is no strong bootstrap support for an animal-plant clade. These results indicate that the animal WDR5 homologs might function like the human WDR5, but raise a question on biochemical functions of the multiple WDR5 homologs in plants.

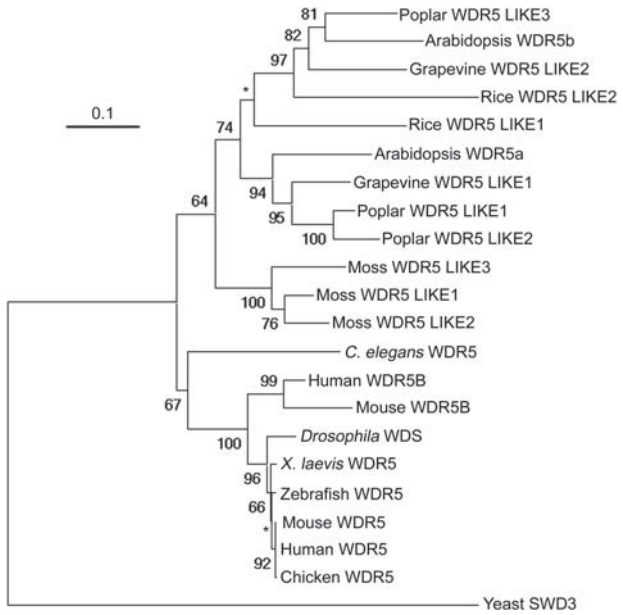

Figure 1. Phylogenetic Tree for WDR5 Homologs from Representative Plant and Animal Species. The tree of full-length WDR5 homologs was constructed by the Neighbor-Joining method using PHYLIP. Bootstrap values are shown for clades with a support greater than 60% (in 1000 sampling replicates). Star indicates a clade without a strong bootstrap support. The protein accession numbers are specified in Table S1.
doi:10.1371/journal.pgen.1001330.g001

RBL Promotes the Expression of *FLC* and *FLC* Homologs to Repress the Floral Transition

It was of great interest to determine biological functions of *ASH2R* and *RBL*. First, we employed a double-stranded RNA interference (dsRNAi) approach to knock down *RBL* expression in wildtype Col (knockout mutants in *RBL* were not publically available). Briefly, a 245-bp *RBL*-specific fragment from the 3′ transcribed region was used to create a dsRNAi cassette driven by the constitutive *35S* promoter. Eight independent transgenic lines were generated, from which homozygous *RBL RNAi-1* and *RBL RNAi-2* lines with a single *T-DNA* locus, were identified. In long days (LD), five out of the eight lines flowered earlier than parental Col, but otherwise were normal; no noticeable phenotypes were observed in the remaining three lines (Figure 2A and 2B, and data not shown). *RBL* transcript levels were quantified in *RBL RNAi-1* and *-2* seedlings by real-time quantitative PCR, and indeed, *RBL* expression was knocked down compared to Col (Figure 2C). Together, these results show that *RBL* represses the floral transition.

FLC plays a central role in floral repression in *Arabidopsis*, and as described in the Introduction, several components involved in H3K4 methylation promote *FLC* expression. Hence, it was of interest to examine whether *FLC* expression was suppressed upon *RBL* knockdown. *FLC* transcript levels were reduced in *RBL RNAi* seedlings compared to Col (Figure 2D). We further examined the expression of *FLC* homologs upon *RBL* knockdown, and found that *MAF4* and *MAF5* transcript levels were reduced, whereas levels of *FLM*, *MAF2* and *MAF3* transcripts in the *RBL RNAi* lines were similar to those in Col (Figure 2D). Together, these results suggest that *RBL* promotes the expression of *FLC*, *MAF4* and *MAF5*, but not *FLM*, *MAF2* or *MAF3*, to repress the floral transition.

ASH2R Represses Flowering and Is Essential for Seed Development

To explore the biological function of *ASH2R*, we identified an *ash2r-1*/+ heterozygous line from the SAIL collection [39], which carries an insertional *T-DNA* in the middle of *ASH2R*. We did not recover any *ash2r-1* homozygotes from a large population of the selfed progeny of *ash2r-1*/+ heterozygotes. Subsequently, we found that in developing siliques from *ash2r-1*/+ plants, about one-fifth of the seeds (167 out of 788 seeds) were aborted white and brown seeds (Figure S3A), whereas in wild-type siliques only less than four thousandth of the seeds (3 out of 798) were aborted. Thus, we conclude that *ash2r-1* homozygous seeds are not viable. Next, we examined *ash2r-1* embryo development under a differential-interference-contrast microscope. Up to globular stage, *ash2r-1* embryos developed similarly as wild-type ones, however, their further development was arrested (Figure S3B-S3H). When wild-type embryos reached heart stage (around 6 days after pollination; DAP), the *ash2r-1* embryos were still at globular stage (Figure S3E and S3H). These findings are in line with a very recent study by Aquea *et al.* [38] showing that *ASH2R/TRO* is essential for *Arabidopsis* early embryogenesis.

To explore the role of *ASH2R* in vegetative development, we exploited a dsRNAi approach to knock down *ASH2R* expression. A 223-bp *ASH2R*-specific fragment was used to create a dsRNAi cassette driven by the *35S* promoter. Four independent homozy-

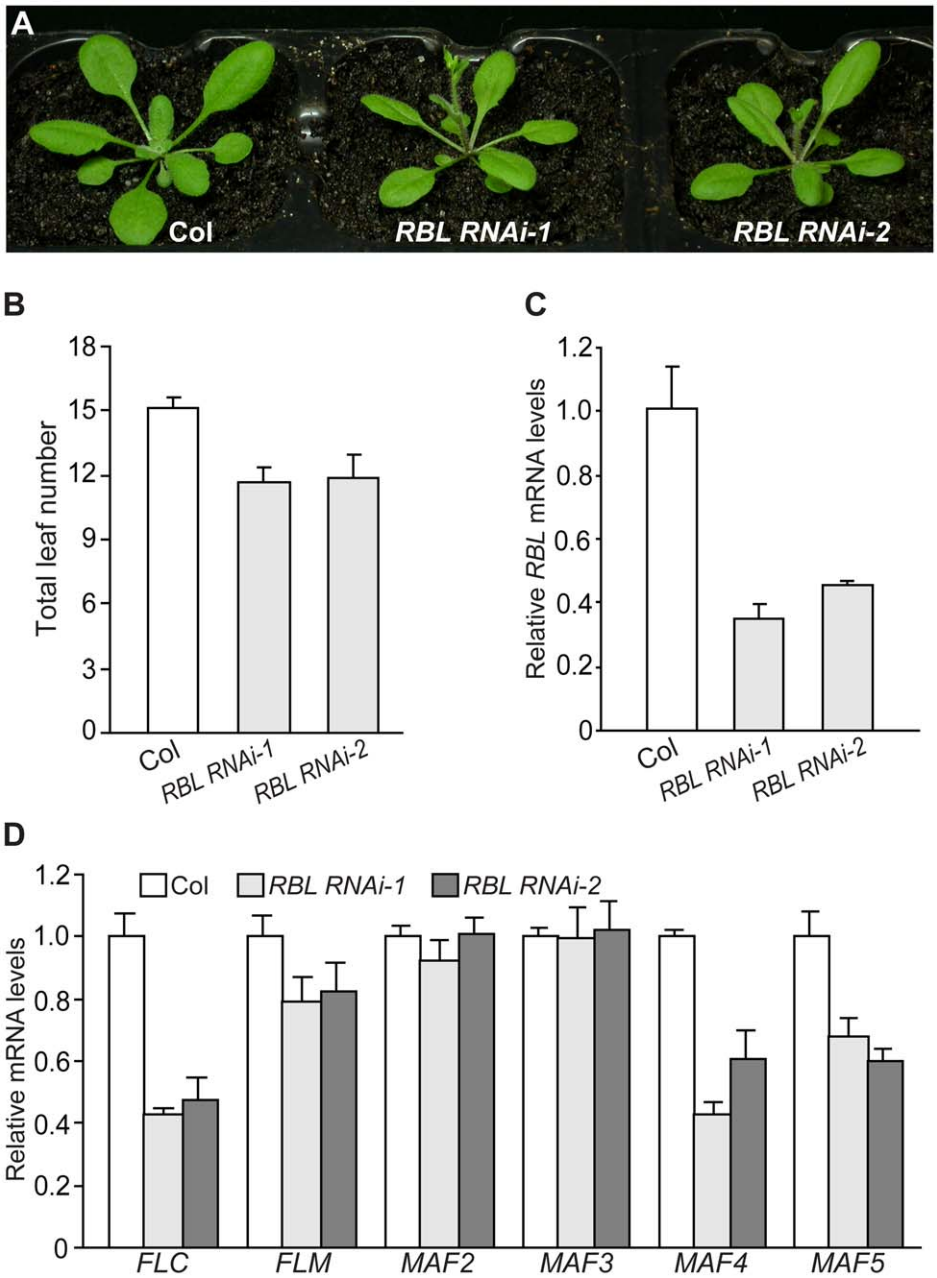

Figure 2. *RBL* Represses the Floral Transition in *Arabidopsis*. (A) Phenotypes of *RBL RNAi* lines grown in long days (LD). Col was used as the parental accession in *RBL* knockdown. (B) Flowering times of the *RBL RNAi* lines grown in LD. The total number of primary rosette and cauline leaves formed prior to bolting was counted, and 11–12 plants were scored for each line. Error bars indicate standard deviations (SD). (C) Relative *RBL* mRNA levels in seedlings of the *RBL RNAi* lines determined by real-time quantitative PCR. Relative expression to parental Col is presented. Bars indicate SD. (D) Relative mRNA levels of *FLC* and *FLC* homologs in *RBL RNAi* seedlings quantified by real-time PCR.
doi:10.1371/journal.pgen.1001330.g002

gous transgenic lines with a single *T-DNA* locus, *ASH2R RNAi-1* to *-4*, were created. These lines all flowered earlier than Col, but otherwise were normal in LD (Figure 3A, 3B). In addition, these lines set seeds normally. *ASH2R* expression was examined in *ASH2R RNAi* seedlings; indeed, it was knocked down and the *ASH2R* transcript levels in these lines were about 30–50% of those in Col (Figure 3C). Furthermore, we quantified the transcript levels of *FLC* and *FLC* homologs in these *RNAi* lines, and found that *FLC*, *MAF4* and *MAF5* expression was reduced, whereas *FLM*, *MAF2* and *MAF3* expression was not affected upon *ASH2R* knockdown (Figure 3D). Thus, *ASH2R*, like *RBL*, is required for the expression of *FLC*, *MAF4* and *MAF5* and represses *Arabidopsis* flowering.

ASH2R Is Required for Normal Leaf Growth and Development

We further investigated the role for *ASH2R* in vegetative development using two mutant lines in which *ASH2R* function is severely disrupted as detailed below. In an effort to create glucocorticoid-inducible *ASH2R* expression lines, we unintentionally introduced two point mutations T_{136} to A and K_{187} to R, into the *ASH2R* coding sequence. Phylogenetic analysis suggests that

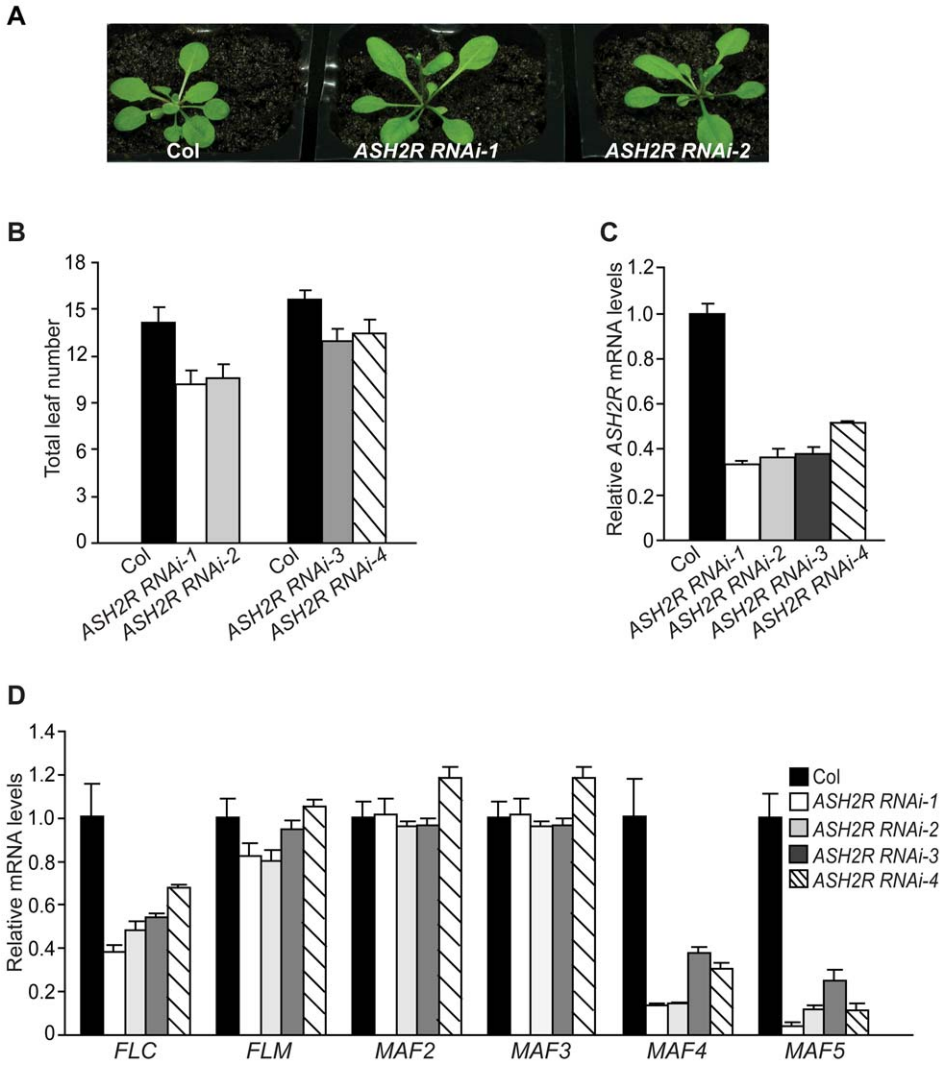

Figure 3. *ASH2R* Knockdown Causes Early Flowering. (A) Phenotypes of *ASH2R RNAi* lines grown in LD. (B) Flowering times of the *ASH2R RNAi* lines grown in LD. Total leaf number for each line (12 plants per line) was counted. Error bars indicate SD. (C) Relative *ASH2R* mRNA levels in *ASH2R RNAi* seedlings determined by real-time quantitative PCR. Relative expression to parental Col is presented. Bars indicate SD. (D) Relative mRNA levels of *FLC* and *FLC* homologs in *ASH2R RNAi* seedlings determined by real-time quantitative PCR. Bars indicate SD.
doi:10.1371/journal.pgen.1001330.g003

T136 is conserved among Ash2 relatives in eudicots, whereas K187 appears not to be conserved (Figure S4B). The point-mutated *ASH2R* transgene was inserted downstream a synthetic promoter known as *pOp6* (Figure S4A), which is responsive to glucocorticoid treatment [40]. In the absence of glucocorticoid induction, we identified five independent lines homozygous for the null *ash2r-1* mutation and carrying the point-mutated *ASH2R* transgene, in which the transgene expression is leaky (see description below).

Individual T_3 populations for these five lines were obtained (note that only transgenic progeny can grow into seedlings due to the embryo lethality of *ash2r-1*); subsequently, we examined a representative T_3 population from each line phenotypically, and found that at seedling stage two lines (Near-Normal #1 and #2) developed like wildtype Col (WT), whereas the other three lines including *ash2r-2* (hypomorphic; thereafter *ash2r-2^{hyp}*) and *ash2r-3* (hypomorphic; thereafter *ash2r-3^{hyp}*) displayed leaf abnormalities (Figure 4A, and data not shown). Of note, all of the progeny within each examined population displayed nearly identical phenotypes that were stably inheritable. In terms of flowering time, the two near normal lines flowered moderately earlier than Col, whereas the other three mutant lines flowered much earlier than Col in LD (Figure 4B, and data not shown). Using real-time quantitative PCR, we further examined *ASH2R* transgene expression in shoot apices from 10-day (d) old seedlings, and found that the *ASH2R* transcript levels in both near-normal lines were higher than those in Col, whereas they were much lower in *ash2r-2^{hyp}* and *-3^{hyp}* compared to Col (Figure 4C). This suggests that the increased transcript levels of point-mutated *ASH2R* can partly ameliorate the partial functionality of point-mutated *ASH2R*. Interestingly, in all of these five lines the *ASH2R* transgene was expressed in the absence of the chemical inducers glucocorticoids; most likely this is because the strong *35S* promoter located at the 3′ end of *ASH2R* may promote its expression (Figure S4A).

To confirm that the early-flowering phenotypes of *ash2r-2^{hyp}* and *-3^{hyp}*, like those of the *ASH2R RNAi* lines, were caused by reduced expression of *FLC* and its homologs, we quantified the transcript levels of *FLC*, *MAF4* and *MAF5* in shoot apices of these lines.

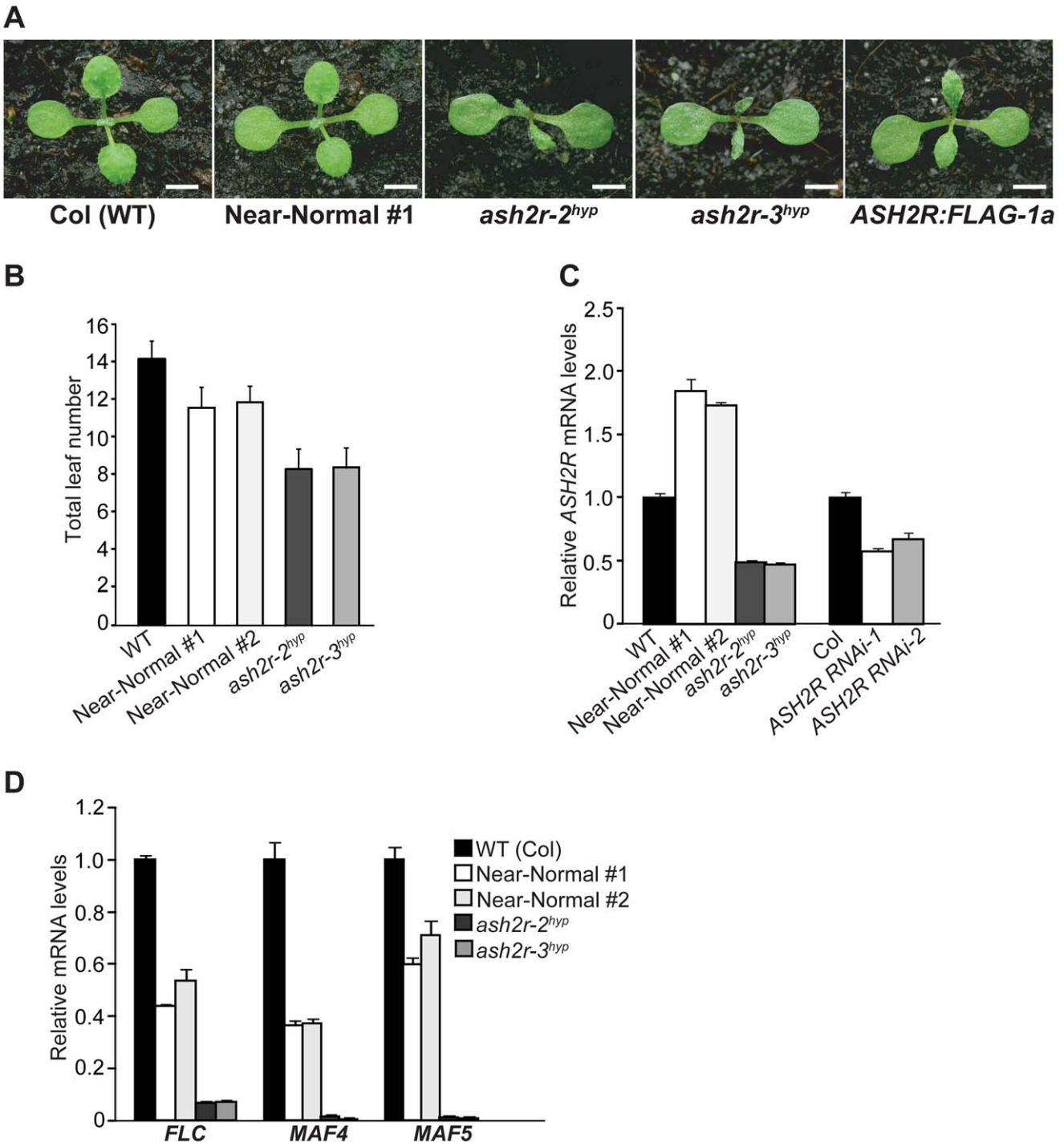

Figure 4. Characterization of the Hypomorphic *ash2r* Mutants. (A) Phenotypes of the hypomorphic *ash2r* mutant seedlings (T_3 generation) grown in LD. On the right is an *ASH2R:FLAG-1a* (T_3) seedling with a leaf phenotype. Bars indicate 2.0 mm. (B) Flowering times of the hypomorphic *ash2r* mutants grown in LD. For each line, 12–15 plants were scored. Error bars indicate SD. (C) Relative mRNA levels of the *ASH2R* transgene in the shoot apices of 10-d-old seedlings of the indicated lines. The transcript levels were determined by real-time quantitative PCR. Relative expression to wildtype Col is presented. Bars indicate SD. (D) Relative mRNA levels of *FLC*, *MAF4* and *MAF5* in the shoot apices of 10-d-old seedlings of the indicated lines.

doi:10.1371/journal.pgen.1001330.g004

Indeed, *FLC* expression was greatly reduced, and both *MAF4* and *MAF5* expression was nearly eliminated in *ash2r-2^{hyp}* and *-3^{hyp}* compared to Col (Figure 4D). Furthermore, we found that only about two-fifth of the siliques or silique-like structures of *ash2r-2^{hyp}* and *-3^{hyp}* bore seeds (typically only several viable seeds in each of these siliques) (Figure S5). As described earlier in the text, the *ASH2R RNAi* lines, unlike *ash2r-2^{hyp}* and *-3^{hyp}*, are normal except for early flowering as *ASH2R* expression is only partially suppressed in the *RNAi* lines. Together, these observations led us to conclude that both *ash2r-2^{hyp}* and *-3^{hyp}* are strong hypomorphic

loss-of-function mutants, largely resulting from the point mutations of T_{136} to A and/or K_{187} to R and an expression reduction in the point-mutated *ASH2R*.

The role of *ASH2R* in leaf growth and development was further explored. We observed that all of the *ash2r-2^{hyp}* and *-3^{hyp}* mutants (T_3) displayed leaf abnormalities: small, narrow, and sometimes curled leaf blades compared to wildtype Col (Figure 4A), suggesting that *ASH2R* is required for proper leaf growth and development. In an effort to create transgenic lines with the *FLAG*-tagged *ASH2R* transgene (*ASH2R:FLAG*), we identified one line named as *ASH2R:FLAG-1a* (T_3 generation) homozygous for the null *ash2r-1* mutation and carrying a single-locus *ASH2R:FLAG* fusion driven by the *35S* promoter. The majority of *ASH2R:FLAG-1a* (T_3) seedlings were near normal as Col, but about one-third of them displayed leaf phenotypes: typically small and narrow leaf blades as exemplified in Figure 4A. These phenotypes were due to the partial functionality of ASH2R:FLAG, not caused by the increased levels of *ASH2R:FLAG* because *ASH2R* overexpression did not give rise to any leaf phenotypes (see Figure 5A, next section). The leaf phenotype of *ASH2R:FLAG-1a* was similar to, but typically weaker than that of the strong hypomorphic *ash2r-2^{hyp}* and *-3^{hyp}* (Figure 4A). Together, these findings demonstrate that besides flowering repression and seed development, *ASH2R* is also required for proper leaf growth and development.

Gain of *ASH2R* Function Activates the Expression of Its Target Genes *FLC*, *MAF4*, and *MAF5* to Delay Flowering

Loss of *ASH2R* function in vegetative development causes accelerated floral transition and leaf abnormalities. We sought to further explore the effects of gain of *ASH2R* function on *Arabidopsis* development. *ASH2R* coding region was overexpressed by the constitutive *35S* promoter in Col. Eight independent transgenic lines were generated, among which three homozygous lines (T_3 generation) with a single *T-DNA* locus, *ASH2Rox-1* to *-3* were further characterized. First, we confirmed that indeed *ASH2R* mRNA levels in these *ASH2Rox* lines were higher than those in parental Col (Figure S6). In opposite to the *ASH2R RNAi* lines, these three lines flowered later than Col (Figure 5A, 5B). In addition, we also observed that three out of the other five lines flowered later than Col (data not shown). Of note, except late flowering, these lines developed normally at vegetative phase (Figure 5A), and no noticeable phenotypes were observed in seed development. We further quantified transcript levels of *FLC* and its homologs in *ASH2Rox* seedlings. In opposite to *ASH2R* knockdown, both *FLC* and *MAF4* expression was upregulated in the *ASH2Rox* lines, and surprisingly, *MAF5* expression was significantly activated upon *ASH2R* overexpression (Figure 5C, 5D). Consistent with that *ASH2R* is not involved in the regulation of *FLM*, *MAF2* and *MAF3*, their transcript levels in the *ASH2Rox* lines were similar to those in Col (Figure 5C and data not shown). Taken together, these results show that *ASH2R* plays an important role in activation of the expression of *FLC*, *MAF4* and *MAF5* to inhibit flowering. Interestingly, the significant activation of *MAF5* expression upon *ASH2R* overexpression appears to have a limited effect on the floral repression. This could be attributed to that *MAF5* may be a weak floral repressor.

The Spatial Expression Patterns of *ASH2R*, *RBL*, and *WDR5a* Overlap in Vegetative and Reproductive Development

It was of interest to examine whether the spatial expression patterns of *ASH2R*, *RBL* and *WDR5a* overlap in vegetative and reproductive phases. To uncover the *ASH2R* spatial pattern, a 1.5-kb 5′ promoter region plus part of the genomic coding region of *ASH2R* was translationally fused with the *β-GLUCURONIDASE* (*GUS*) gene. In addition, a 1.1-kb promoter plus 0.6-kb the genomic coding region of *RBL* was translationally fused with *GUS*. Both transgenes were introduced into Col, and using histochemical staining we found that in vegetative phase both *ASH2R* and *RBL* were strongly expressed in root tips, shoot apices and vascular tissues (Figure 6A). This pattern overlaps with those of *WDR5a* and *FLC* [21,24].

Next, we analyzed the spatial patterns of *ASH2R-GUS*, *RBL-GUS* and *WDR5a-GUS* in seed development. *ASH2R-GUS* was strongly expressed in developing embryos and endosperms (Figure 6C, 6D), consistent with *ASH2R* playing an essential role in seed development. In addition, both *WDR5a* and *RBL*, like *ASH2R*, were expressed in developing embryos and endosperms at globular and heart stages (Figure 6E–6H). Together, these findings are consistent with the notion that ASH2R, RBL and WDR5a might act as part of a complex in vegetative and seed development.

ASH2R and RBL Form a Nuclear Subcomplex with WDR5a, but Not with WDR5b, in Vegetative and Reproductive Development

We further explored whether ASH2R, RBL and WDR5a form a stable complex. First, yeast two-hybrid assays were carried out to examine direct associations among these three proteins. In yeast, ASH2R interacted with RBL, not with WDR5a, whereas RBL interacted with WDR5a (Figure 7A and 7C). Next, to examine whether RBL associated with ASH2R and WDR5a in plant cells, we performed bimolecular fluorescence complementation (BiFC) experiments using non-fluorescent N-terminal and C-terminal EYFP (for Enhanced Yellow Fluorescent Protein) fragments (named as nEYFP and cEYFP, respectively) fused to the full-length WDR5a, ASH2R or RBL proteins. nEYFP-ASH2R and RBL-cEYFP were simultaneously expressed in onion epidermal cells, and fluorescence was observed in the nuclei of onion cells (Figure 7B), demonstrating that ASH2R associates with RBL. Similarly, we also found that RBL associated with WDR5a in the nuclei of onion cells (Figure 7D), consistent with that ASH2R, RBL and WDR5a form a complex.

Our phylogenetic analyses of the WDR5 homologs show that there are multiple WDR5 homologs in land plants (Figure 1). Besides WDR5a, *Arabidopsis* has another WDR5 homolog, WDR5b. We sought to determine whether WDR5b could form a complex with RBL and ASH2R. Using yeast two-hybrid approach, surprisingly, we found that WDR5b did not interact with either RBL or ASH2R in yeast (Figure S7). These results suggest that in *Arabidopsis* there may be only a single core subcomplex for H3K4 methylation, namely ASH2R-RBL-WDR5a.

We further performed co-immunoprecipitation experiments to determine if ASH2R, RBL and WDR5a form a complex *in vivo* using the *ASH2R:FLAG-1a* line (T_3). Indeed, anti-FLAG specifically immunoprecipitated WDR5a from young seedlings and developing siliques (Figure 7E–7F). As described above, ASH2R physically associates with RBL which directly associates with WDR5a (Figure 7B and 7D), and there is no direct association between ASH2R and WDR5a (Figure 7C). Thus, ASH2R may form a complex with WDR5a via RBL. To determine whether RBL is required for the *in vivo* complex formation of ASH2R with WDR5a, we crossed the *RBL RNAi-1* into the *ASH2R:FLAG-1a* line, and subsequently, the F_1 seedlings were used for co-immunoprecipitation. Upon *RBL* knockdown, the anti-FLAG recognizing ASH2R:FLAG failed to pull down WDR5a in *RBL RNAi-1;ASH2R:FLAG-1a* seedlings (Figure 7G). Thus, RBL is

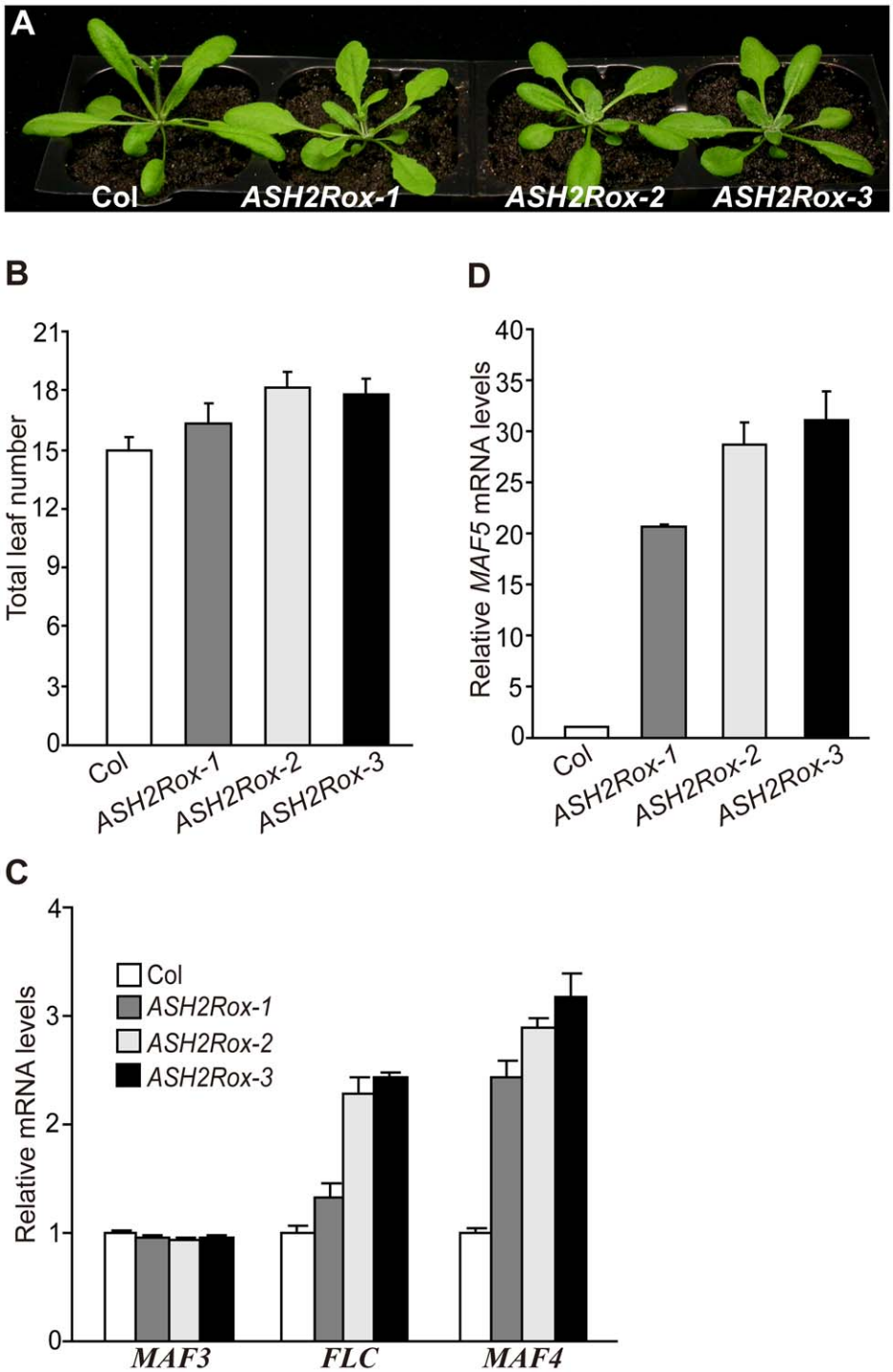

Figure 5. Overexpression of *ASH2R* Activates the Expression of *FLC, MAF4,* and *MAF5* to Delay Flowering. (A) Phenotypes of *ASH2R* overexpression lines grown in LD. (B) Flowering times of *ASH2Rox* lines grown in LD. Total leaf number at flowering for each line (11 plants per line) was counted. Error bars indicate SD. (C) Relative mRNA levels of *FLC, MAF3* and *MAF4* in *ASH2Rox* and Col seedlings determined by real-time quantitative PCR. Relative expression to parental Col is presented. Bars indicate SD. (D) Relative *MAF5* mRNA levels in *ASH2Rox* and Col seedlings.
doi:10.1371/journal.pgen.1001330.g005

required for the ASH2R-WDR5a complex formation. These results together led us to conclude that ASH2R, RBL and WDR5a form a complex during vegetative and reproductive development.

The physical association of RBL with ASH2R and WDR5a in the onion nuclei suggests that the ASH2R-RBL-WDR5a complex acts in the nucleus. Recently, it has been reported that a transiently expressed fusion protein of ASH2R with GFP (for Green Fluorescent Protein) in onion cells is localized into the nucleus [38]. Using an *ASH2R-GFP* transgenic line, we confirmed that the ASH2R fusion protein was indeed localized specifically in the nucleus (Figure S8). Together, these results are consistent with that the ASH2R subcomplex functions as a transcriptional regulator.

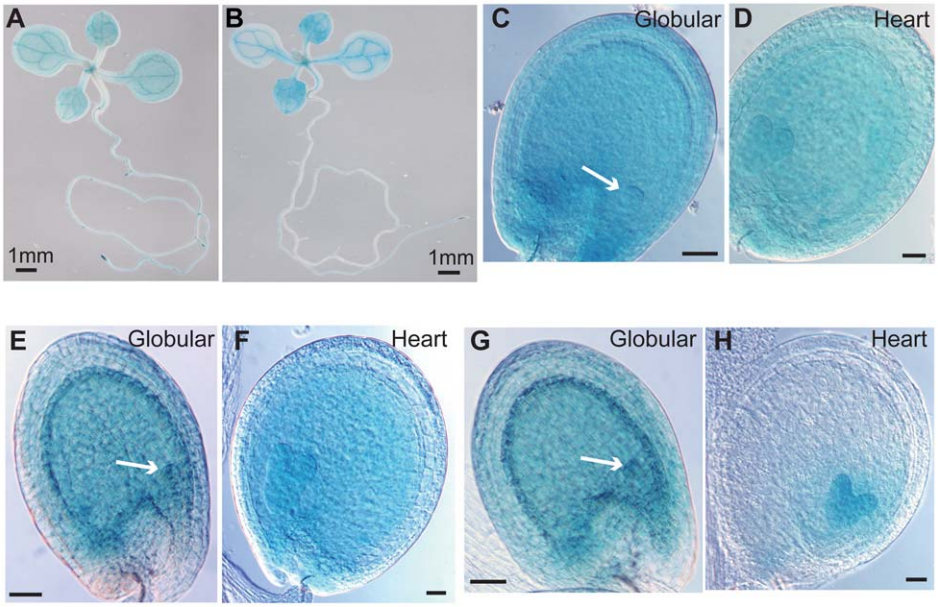

Figure 6. Spatial Expression Patterns of *ASH2R*, *RBL*, and *WDR5a*. (A–B) *ASH2R-GUS* (A) and *RBL-GUS* (B) expression in 1-week-old seedlings. (C–D) *ASH2R-GUS* expression in a representative seed with globular embryo indicated by an arrow (C), and with heart embryo (D). (E–F) *RBL-GUS* expression in a representative seed with globular embryo (E), and with heart embryo (F). (G–H) *WDR5a-GUS* expression in a representative seed with globular embryo (G), and with heart embryo (H). (C–H) Bars = 50 μm.
doi:10.1371/journal.pgen.1001330.g006

WDR5a Protein Interacts with Multiple Putative *Arabidopsis* H3K4 Methyltransferases

The human Ash2-RbBP5-WDR5 core subcomplex associates with MLL1, MLL2 and other H3K4 methyltransferases to form distinct catalytic complexes that deposit both di- and tri-methyl H3K4 [9,10,41,42]. In *Arabidopsis* genome, there are may be up to ten putative H3K4 methyltransferases [17]. Recently we have found that WDR5a can associate with ATX1 [24]. Using yeast two-hybrid approach, we further explored whether WDR5a could associate with other putative H3K4 methyltransferases including SDG14 and SDG16. Full-length SDG14 and SDG16 proteins fused to the GAL4 DNA-Binding Domain (BD) were co-expressed with WDR5a fused to the GAL4 Activation Domain (AD) in yeast, and subsequently, we found that both SDG14 and SDG16 physically interacted with WDR5a (Figure 8A and 8C). Next, using BiFC we examined whether WDR5a could interact with SDG14 and SDG16 in plant cells. Upon simultaneous expression of WDR5a-cEYFP with nEYFP-SDG14 or nEYFP-SDG16 in onion epidermal cells, fluorescence was observed in the nuclei (Figure 8B and 8D). Hence, WDR5a indeed can physically interact with SDG14 and SDG16 in plant cells. In addition, we found that neither RBL nor ASH2R interacted with SDG14, SDG16 or ATX1 (Figure S9). Based on these results, we infer that the ASH2-RBL-WDR5a subcomplex associates with different H3K4 methyltransferases via WDR5a to form multiple functional COMPASS-like H3K4 methyltransferase complexes in *Arabidopsis*.

ASH2R Mediates Genome-Wide Trimethylation, but Not Di- or Mono-Methylation of H3K4

In yeast and mammal cells, Ash2-containing COMPASS and COMPASS-like complexes catalyze di- and tri-methylation of H3K4 [8,9]; removal of BRE2 (the Ash2 homolog) function in yeast causes a great reduction in genome-wide H3K4me2 and H3K4me3 [8]. Recent studies reveal that the deficiency of MLL2 (the H3K4 methyltransferase of MLL2 COMPASS-like complex) in the mouse oocytes leads to a reduction in global H3K4me2 and H3K4me3 [42]. As described above, the *Arabidopsis* ASH2R core subcomplex can associate with multiple putative H3K4 methyltransferases to form catalytic COMPASS-like complexes. We sought to investigate the role of *Arabidopsis* ASH2R-COMPASS in H3K4 methylation. First, genome-wide H3K4 methylation was examined upon loss of *ASH2R* function. Total histones were extracted from seedlings of wildtype Col and the strong hypomorphic *ash2r-2*^{hyp} and *-3*^{hyp}, and levels of monomethyl H3K4 (H3K4me1), H3K4me2 and H3K4me3 were measured by western blotting with antibodies specifically recognizing these modifications. We found that H3K4me3, but surprisingly not H3K4me2, was strongly reduced upon loss of *ASH2R* function (Figure 9A). In addition, H3K4 monomethylation was not affected in *ash2r-2*^{hyp} or *-3*^{hyp} compared to the wildtype (Figure 9A). Next, we examined global H3K4 methylation in *ASH2R*-overexpression seedlings including *ASH2Rox-2* and *-3*, and found that in opposite to loss of *ASH2R* function, H3K4me3 levels were increased in both *ASH2Rox-2* and *-3* lines, whereas levels of H3K4me1 and H3K4me2 remained unchanged compared to parental Col (Figure 9B, 9C). Together, these results suggest that in *Arabidopsis*, the ASH2R-COMPASS complexes are responsible for H3K4 trimethylation, but not for di- or mono-methylation of H3K4.

ASH2R Binds to the Chromatin of Its Target Genes and Mediates Tri-, but Not Di- Methylation of H3K4 in These Loci

To investigate whether ASH2R directly interacted with its target the *FLC* locus to activate its expression, we performed chromatin immunoprecipitation (ChIP) with anti-FLAG using the wildtype-like seedlings of *ASH2R:FLAG-1a* (T_3) in which *FLC* expression was only moderately suppressed (*FLC* transcript levels in *ASH2R:FLAG-1a* WT-like seedlings were about 60% of those in Col). ASH2R was enriched around the *FLC* TSS (*FLC-P*), but not in a distal region upstream of the TSS (*FLC-U*) or in the middle of

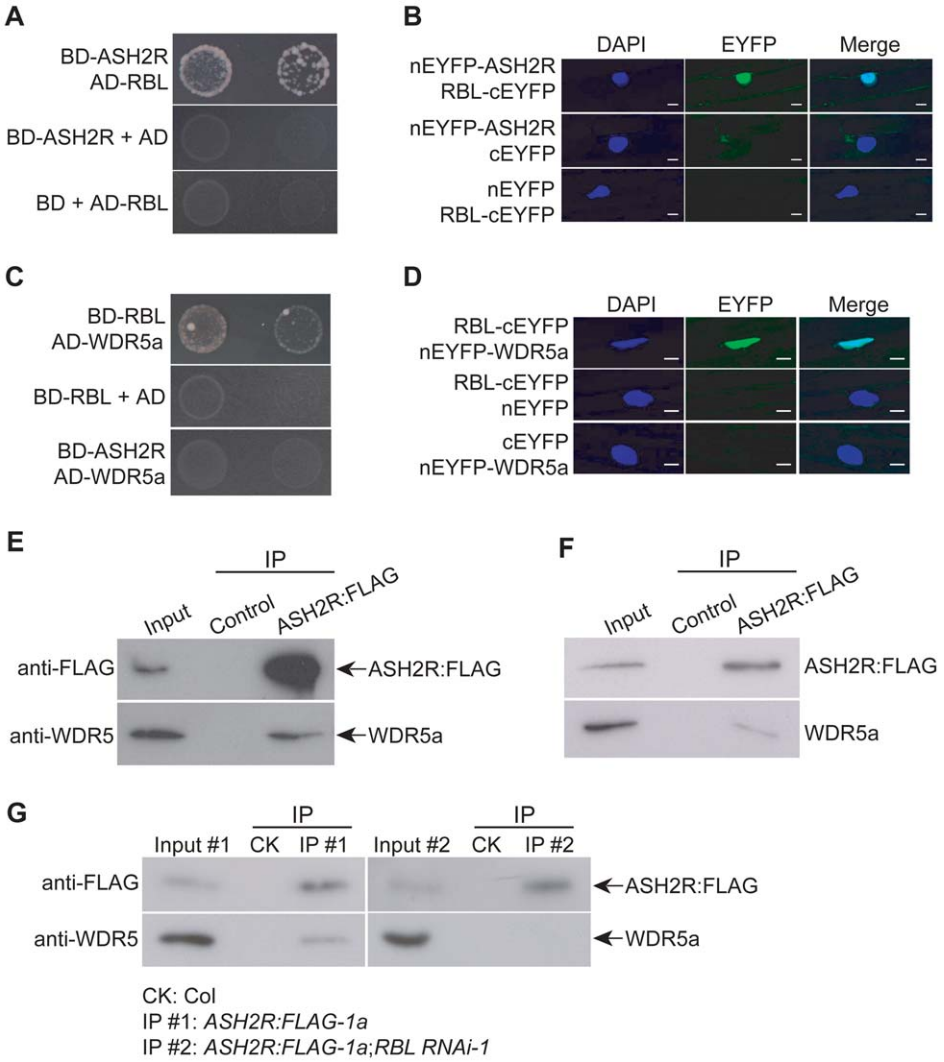

Figure 7. ASH2R, RBL, and WDR5a Form a Nuclear Complex during Vegetative and Reproductive Development. (A) Interaction of ASH2R with RBL in yeast. Full-length ASH2R and RBL proteins were respectively fused with the GAL4 DNA-binding domain (BD) and activation domain (AD). Yeast cells harboring these fusions, AD and/or BD, as indicated, were grown on the highly selective SD media lacking of Trp, Leu, His and adenine. (B) BiFC assay of nEYFP-ASH2R and RBL-cEYFP in onion epidermal cells. Plasmid pairs as indicated, were used to transiently co-transform onion epidermal cells by biolistic gene bombardment. Yellowish-green signal indicates the binding of nEYFP-ASH2R with RBL-cEYFP in the nuclei. Blue fluorescence from DAPI (4′,6-diamidino-2-phenylindole) staining indicates nuclei. Fluorescence signals were imaged using a laser scanning confocal microscope. Bar = 20 μm. (C) Interaction of WDR5a with RBL in yeast. Full-length WDR5a and RBL proteins were fused with the GAL4 BD and AD domains, respectively. (D) Physical interaction of WDR5a with RBL in onion epidermal cells as analyzed by BiFC. Bar = 20 μm. (E) Co-immunoprecipitation of ASH2R with WDR5a in 10-d-old seedlings. Total protein extracts from Col (WT; as a negative control) and *ASH2R:FLAG-1a* (T_3) seedlings were immunoprecipitated with anti-FLAG agarose, and subsequently, the precipitates were analyzed by western blotting with anti-FLAG and anti-WDR5. The input was the *ASH2R:FLAG-1a* protein extract. (F) Co-immunoprecipitation of ASH2R with WDR5a in 5-DAP *ASH2R:FLAG-1a* siliques (T_3). The input was the *ASH2R:FLAG-1a* protein extract from siliques. (G) Co-immunoprecipitation analysis of ASH2R with WDR5a upon *RBL* knockdown. Total protein extracts from the seedlings of Col (as a negative control), hemizygous *ASH2R:FLAG-1a* (from the crossing of *ASH2R:FLAG-1a* to Col), and doubly hemizygous *RBL RNAi-1;ASH2R:FLAG-1a* were immunoprecipitated with anti-FLAG agarose. Input #1 and Input #2 were the protein extracts of *ASH2R:FLAG-1a* and *RBL RNAi-1;ASH2R:FLAG-1a*, respectively.
doi:10.1371/journal.pgen.1001330.g007

FLC (*FLC-M*) (Figure 10B). Thus, we infer that the ASH2R core subcomplex directly binds to *FLC* chromatin to regulate its expression.

Next, we investigated the effect of *ASH2R* knockdown on di- and tri-methylation of H3K4 in *FLC* chromatin in *ASH2R RNAi* seedlings by ChIP. Previously, it has been shown that H3K4 trimethylation predominantly occurs around the TSS in the actively transcribed *FLC* locus [13,21]. We found that upon *ASH2R* knockdown, H3K4me3 levels were reduced in the *FLC TSS* region (Figure 10C), consistent with the ASH2R binding to this region. Furthermore, we found that levels of H3K4me2 in *FLC* chromatin remained unchanged upon *ASH2R* knockdown (Figure 10D). Hence, *ASH2R* is required for H3K4me3, but not for H3K4me2 in *FLC* chromatin, in line with that ASH2R mediates only genome-wide trimethylation, but not dimethylation of H3K4.

We further examined the association of ASH2R with the *MAF4* and *MAF5* loci, and found that ASH2R bound to the chromatin of 5′ transcribed regions of both *MAF4* and *MAF5*, but not to the 5′ region of *MAF3* that is located immediately upstream of *MAF4*

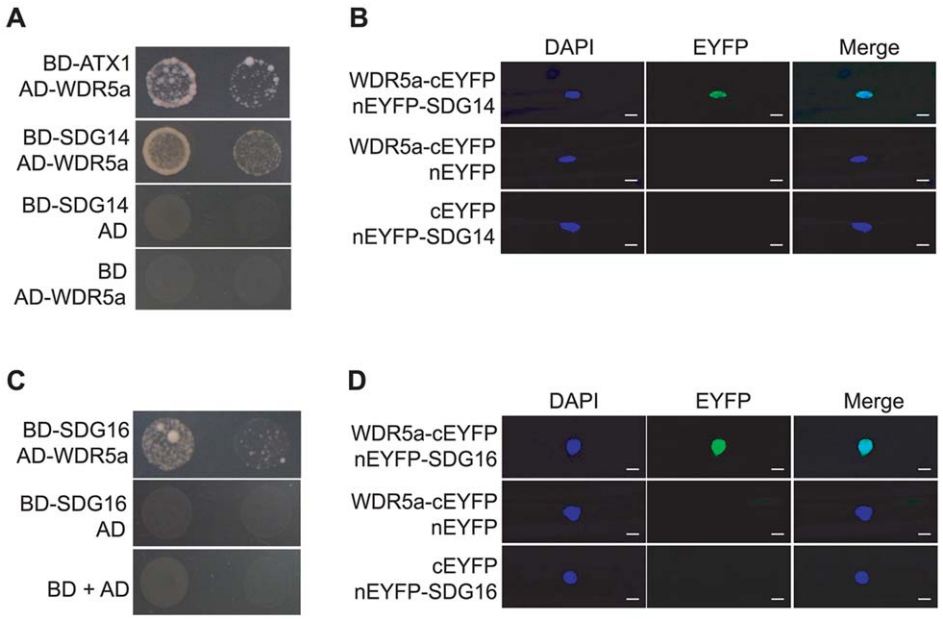

Figure 8. WDR5a Associates with Multiple Putative H3K4 Methyltransferases. (A) Interaction of WDR5a with SDG14 in yeast. Full-length WDR5a and SDG14 proteins were respectively fused with the GAL4 AD and BD domains. Yeast cells harboring these fusions, AD and/or BD, as indicated, were grown on the highly selective SD media lacking of Trp, Leu, His and adenine. (B) Physical interaction of WDR5a-cEYFP with nEYFP-SDG14 in onion epidermal cells as analyzed by BiFC. Yellowish-green signal indicates the binding of WDR5a-cEYFP with nEYFP-SDG14 in the nuclei. Blue DAPI staining indicates nuclei. Bar = 20 μm. (C)Association of WDR5a with SDG16 in yeast. Full-length WDR5a and SDG16 proteins were respectively fused with the GAL4 AD and BD domains. (D) Physical interaction of WDR5a-cEYFP with nEYFP-SDG16 in onion epidermal cells analyzed by BiFC. Yellowish-green signal indicates the binding of WDR5a-cEYFP with nEYFP-SDG16 in the nuclei. Bar = 20 μm.
doi:10.1371/journal.pgen.1001330.g008

(Figure 10B), consistent with that *ASH2R* promotes the expression of *MAF4* and *MAF5*, but not *MAF3*. Furthermore, ChIP assays show that levels of H3K4me3 in both *MAF4* and *MAF5* in their 5′ transcribed regions were strongly reduced, whereas H3K4me2 levels remained unchanged in both genes in *ASH2R RNAi* seedlings relative to Col (Figure 10C, 10D). Thus, ASH2R directly mediates H3K4 trimethylation not only in *FLC*, but also in *MAF4* and *MAF5*.

Gain of *ASH2R* Function Causes Elevated H3K4 Trimethylation, but Not H3K4 Dimethylation, in Its Target Genes to Activate Their Expression

As described in Introduction, H3K4 trimethylation is a chromatin mark for actively transcribed eukaryotic genes, but whether H3K4me3 can cause transcriptional activation is unclear. We have found that *ASH2R* overexpression causes activation of *FLC*, *MAF4* and *MAF5* expression. Increased *ASH2R* expression is expected to increase the availability of ASH2R protein for assembly of ASH2R-COMPASS complexes. It was of great interest to determine whether *ASH2R* overexpression would cause elevated H3K4 trimethylation in *FLC*, *MAF4* and *MAF5*, consequently leading to their activation. First, we performed ChIP experiments to examine tri-methyl H3K4 levels in these loci in Col and *ASH2Rox-2* seedlings. At the *FLC* locus, levels of H3K4me3 in *FLC-P*, but not in *FLC-U*, were increased in *ASH2Rox-2* relative to Col (Figure 11A). Interestingly, H3K4me3 levels in *FLC-M* were also increased upon elevated *ASH2R* expression (Figure 11A). In addition, we found that H3K4me3 levels in *MAF4* were increased in *ASH2Rox-2* seedlings relative to Col (Figure 11A). At the *MAF5* locus, a strong increase of H3K4me3 was observed upon *ASH2R* overexpression (Figure 11A). Noteworthily, upon *ASH2R* overexpression in *ASH2Rox-2* seedlings, a two-fold increase of H3K4me3 in *MAF5* chromatin appears to cause an around 30-fold increase in *MAF5* mRNA levels (Figure 5D and Figure 11A), indicating that at the *MAF5* locus, H3K4 trimethylation state exerts a strong effect on its activation.

We further examined H3K4 dimethylation state in *FLC*, *MAF4* and *MAF5*. Consistent with that the ASH2R core subcomplex is required for genome-wide H3K4 trimethylation, but not for H3K4 dimethylation, levels of H3K4me2 in these three loci remained unchanged in *ASH2Rox-2* seedlings compared to Col (Figure 11B). Thus, consistent with ASH2R's role for H3K4 trimethylation, *ASH2R* overexpression leads to increased levels of H3K4me3, but not H3K4me2, in its target genes.

To further explore the role for ASH2R in the promotion of H3K4 trimethylation in its target genes, we carried out timed activations of *ASH2R* expression using a transgenic line (in the Col background) harboring a stringent two-component glucocorticoid-inducible transgene expression system that has been widely used for gene expression induction in plants [40,43]. In this line (harboring *pOp6-ASH2R*;*p35S-GR:LhG4*), the expression of *ASH2R* transgene (free of mutations) was directed by the *pOp6* promoter (Figure S10A), that is recognized by the *trans*-acting transcriptional activator GR:LhG4 (GR for Glucocorticoid Receptor). Upon binding of GR to glucocorticoids such as dexamethasone (DEX), GR:LhG4 is expected to specifically binds to *pOp6* to turn on *ASH2R* expression. As noted earlier, we observed leaky expression of the point-mutated *ASH2R* transgene, likely caused by proximity of the *35S* promoter driving *GR:LhG4* expression; hence, we re-oriented *p35S* to maximize its distance to *pOp6* (Figure S10A). Because *ASH2R* expression levels exert a much stronger effect on *MAF5* expression than on *FLC* or *MAF4* expression (Figure 5C, 5D), we followed *MAF5* induction upon DEX-activated *ASH2R* expression as described next. We applied DEX to 7-d-old seedlings, and found that with a single application, *MAF5* expression was slightly induced in 72 hour (h) (Figure S10C).

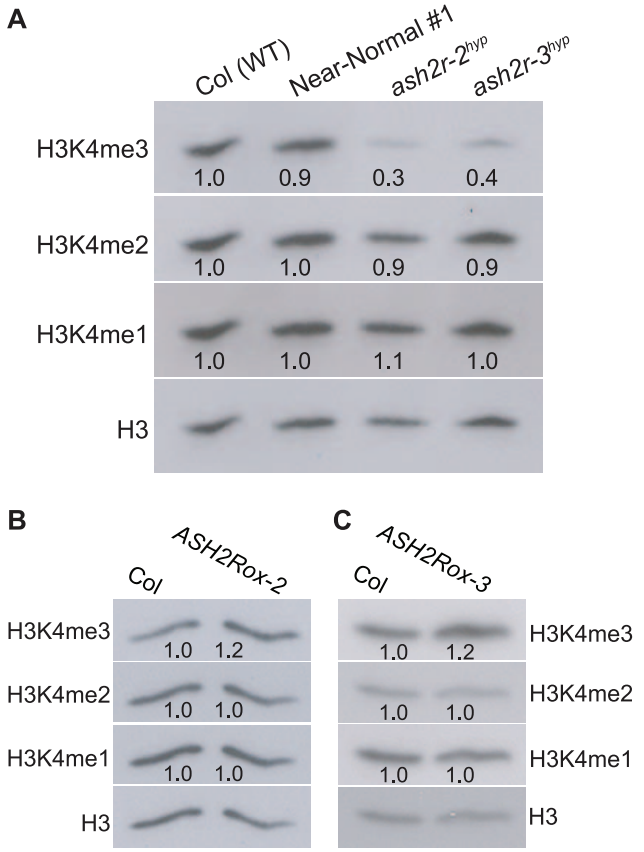

Figure 9. Analyses of Genome-Wide H3K4 Methylation upon Loss of *ASH2R* Function or *ASH2R* Overexpression. (A) Loss of *ASH2R* function causes a strong reduction in global H3K4me3, but not H3K4me2 or H3K4me1. Total histones were extracted from 10-d-old seedlings of Col (WT) and the strong hypomorphic *ash2r-2*^{hyp} and *-3*^{hyp}, and subsequently were analyzed by western blotting. Total H3 in each sample serves as a loading control. The intensity of each protein band was quantified with the Quantity One software, and subsequently, was normalized to total H3. Values are fold changes of *ash2r-2*^{hyp} or *ash2r-3*^{hyp} over WT. (B–C) Analysis of levels of global H3K4me1, H3K4me2 and H3K4me3 in the *ASH2R* overexpression lines *ASH2Rox-2* and *-3*. Total histones were extracted from 10-d-old seedlings of Col, *ASH2Rox-2* and *ASH2Rox-3*, and subsequently, were analyzed by western blotting.
doi:10.1371/journal.pgen.1001330.g009

Next, we applied DEX twice (the second application occurred 36h after the initial treatment); *ASH2R* expression was strongly activated upon DEX applications (still up to about 20 fold in 96h; see Figure 11C). Following *ASH2R* expression activation, *MAF5* expression in shoot apices including newly emerged leaves, was induced to 2.0 fold over the mock in 72h and about 4.0 fold in 96h (Figure 11D). In addition, we found that *MAF5* expression was not induced in the first pair of rosette leaves even though *ASH2R* expression was highly activated upon DEX applications (Figure S10D-S10E), suggesting that cell division activity is required for *MAF5* induction. Interestingly, it took at least about 48h to induce *MAF5* expression upon *ASH2R* expression activation (Figure 11D). *Arabidopsis* shoot apical meristematic cells divide once in 1–2 d [44]. It is likely that one to two rounds of cell division (or DNA replication) in the shoot apices may be required for *MAF5* induction by ASH2R.

We performed ChIP experiments to examine H3K4 methylation state in *MAF5* chromatin at 48h and 96h after the initial DEX application. Levels of H3K4me3, but not H3K4me2 in *MAF5*, increased in 96h, consistent with the induction of *MAF5* expression (Figure 11E, 11F). Thus, the timed *ASH2R* induction causes increased H3K4me3 in *MAF5* chromatin and turns on *MAF5* expression. These findings together with the elevated levels of H3K4me3 in *FLC*, *MAF4* and *MAF5* upon *ASH2R* overexpression, strongly suggest that increased H3K4 trimethylation in these loci causes activation of their expression.

Discussion

In this study, we have found that ASH2R and RBL form a core subcomplex with WDR5a, but not WDR5b, which mediates genome-wide H3K4 trimethylation. The ASH2R core subcomplex, in association with H3K4 methyltransferases, mediates H3K4 trimethylation, but not H3K4 dimethylation in its target genes *FLC*, *MAF4* and *MAF5*, resulting in activation of these gene expression, leading to late flowering. In short, our study provides strong evidence for that there are multiple ASH2R-COMPASS complexes in *Arabidopsis*, which deposit H3K4me3, but not H3K4me2 or H3K4me1, and that H3K4me3 accumulation can activate target gene expression in eukaryotes.

COMPASS-Like H3K4 Methyltransferase Complexes and Their Roles for Developmental Processes in *Arabidopsis*

The human COMPASS-like complexes contain three structural core components, one H3K4 methyltransferase and several non-conserved components [2]; the three core components together with the methyltransferase form a functional (catalytic) core complex for H3K4 methylation [10]. In this study, we have found that the *Arabidopsis* ASH2R, RBL and WDR5a, homologs of the three structural core components of the COMPASS-like complexes, form a core subcomplex during vegetative and reproductive development. Although there are two WDR5 homologs in *Arabidopsis*, our study suggests that *Arabidopsis* only has a single core subcomplex for H3K4 methylation, namely ASH2R-RBL-WDR5a. The biochemical and biological functions of WDR5b remain elusive. Our phylogenetic analyses show that in contrast to most animals, there are multiple WDR5 homologs in land plants. Biochemical functions of these proteins cannot be directly inferred simply based on the homology to WDR5, and have to be determined experimentally.

In *Arabidopsis* there are may be up to 10 putative H3K4 methyltransferases based on similarity of the catalytic SET domains to the known H3K4 methyltransferases in yeast and animals. We have found that WDR5a can associate with multiple putative H3K4 methyltransferases including ATX1, SDG14 and SDG16. Thus, we infer that multiple COMPASS-like H3K4 methyltransferase complexes exist in the higher plant *Arabidopsis*, for instance, the ASH2R-RBL-WDR5a-ATX1 complex. Of note, this ASH2R-ATX1 complex might contain other co-components beside the four-component catalytic core complex. These COMPASS-like complexes are expected to methylate H3K4 in various target genes and control multiple developmental processes including leaf growth and development, the floral transition and seed development.

The ASH2R-ATX1 COMPASS-like complex activates *FLC* expression to repress the floral transition in the rapid-cycling accession Col. Recently it has been shown that the ATX1 protein binds to *FLC* chromatin [21]; in this study, we have found that ASH2R, like ATX1, directly interacts with the *FLC* locus. These findings are consistent with that these two proteins are part of the ASH2R-ATX1 complex binding to *FLC* chromatin to activate *FLC* expression. Our genetic analyses show that loss-of-function *ash2r* mutants, similar to *atx1*, cause a great reduction in *FLC*

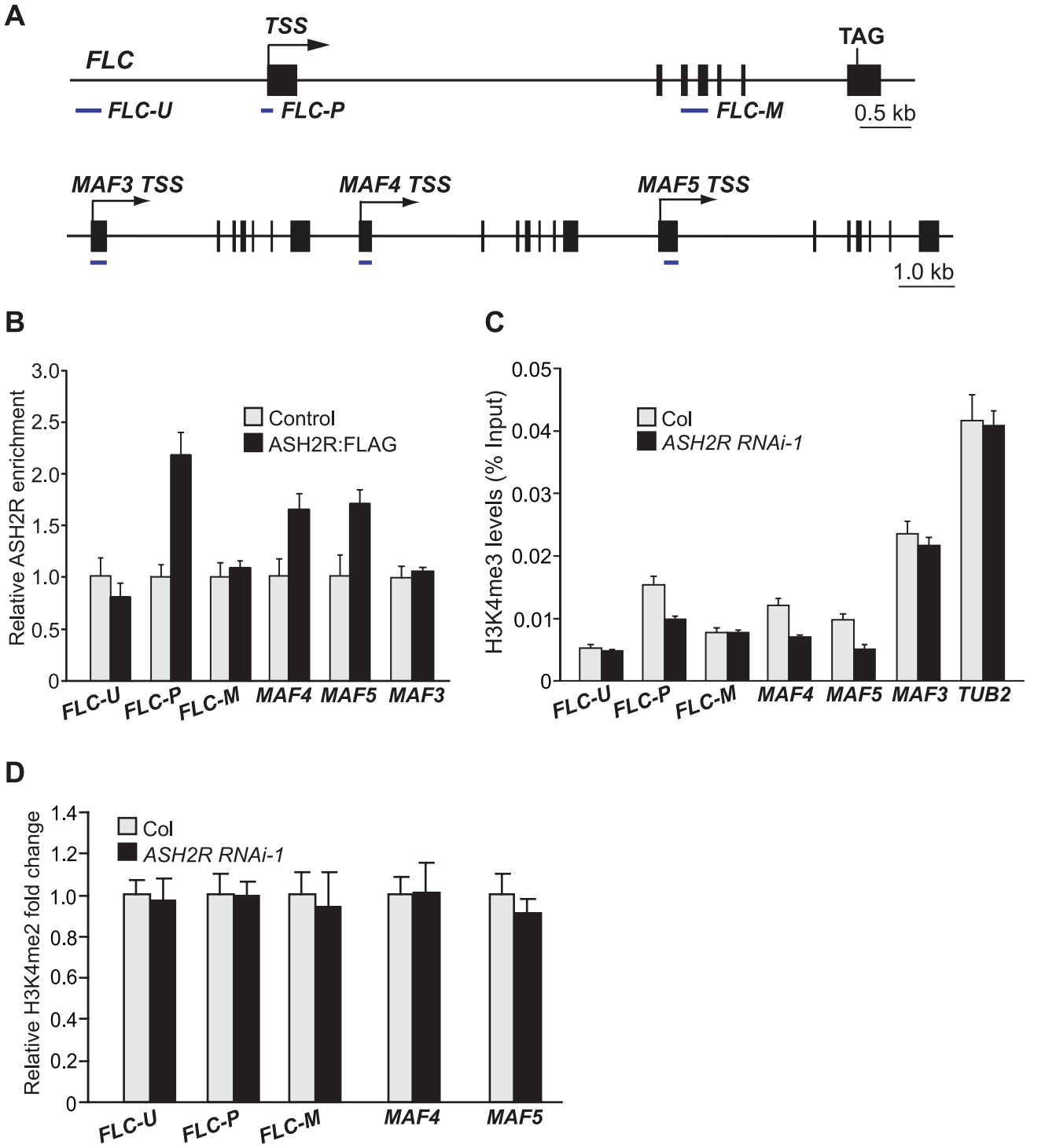

Figure 10. ASH2R Directly Mediates H3K4 Trimethylation in Its Target Genes *FLC*, *MAF4*, and *MAF5*. (A) Schematic structures of *FLC*, *MAF3*, *MAF4* and *MAF5*. The regions examined in ChIP experiments are indicated with solid lines under each region. The transcription start site (TSS) for each gene is indicated by an arrow, and filled boxes for exons. (B) ASH2R enrichment at the *FLC*, *MAF4* and *MAF5* loci. Anti-FLAG was used to immunoprecipitate target chromatin extracted from wildtype-like seedlings of *ASH2R:FLAG-1a* (T_3) or Col (served as control). The amounts of immunoprecipitated genomic fragments were measured by real-time quantitative PCR, and subsequently normalized to *TUBLIN2* (*TUB2*), an internal control. The fold enrichments of the *ASH2R:FLAG* line over control (Col) at the indicated regions are shown. Error bars indicate SD. (C) H3K4me3 levels in *FLC*, *MAF4* and *MAF5* in Col and *ASH2R RNAi-1* seedlings. The amounts of immunoprecipitated genomic fragments were quantified, and subsequently normalized to the input DNA. For each amplicon, the percentage of input is shown. Error bars indicate SD. (D) Analysis of H3K4me2 in *FLC*, *MAF4* and *MAF5* in Col and *ASH2R RNAi-1* seedlings.
doi:10.1371/journal.pgen.1001330.g010

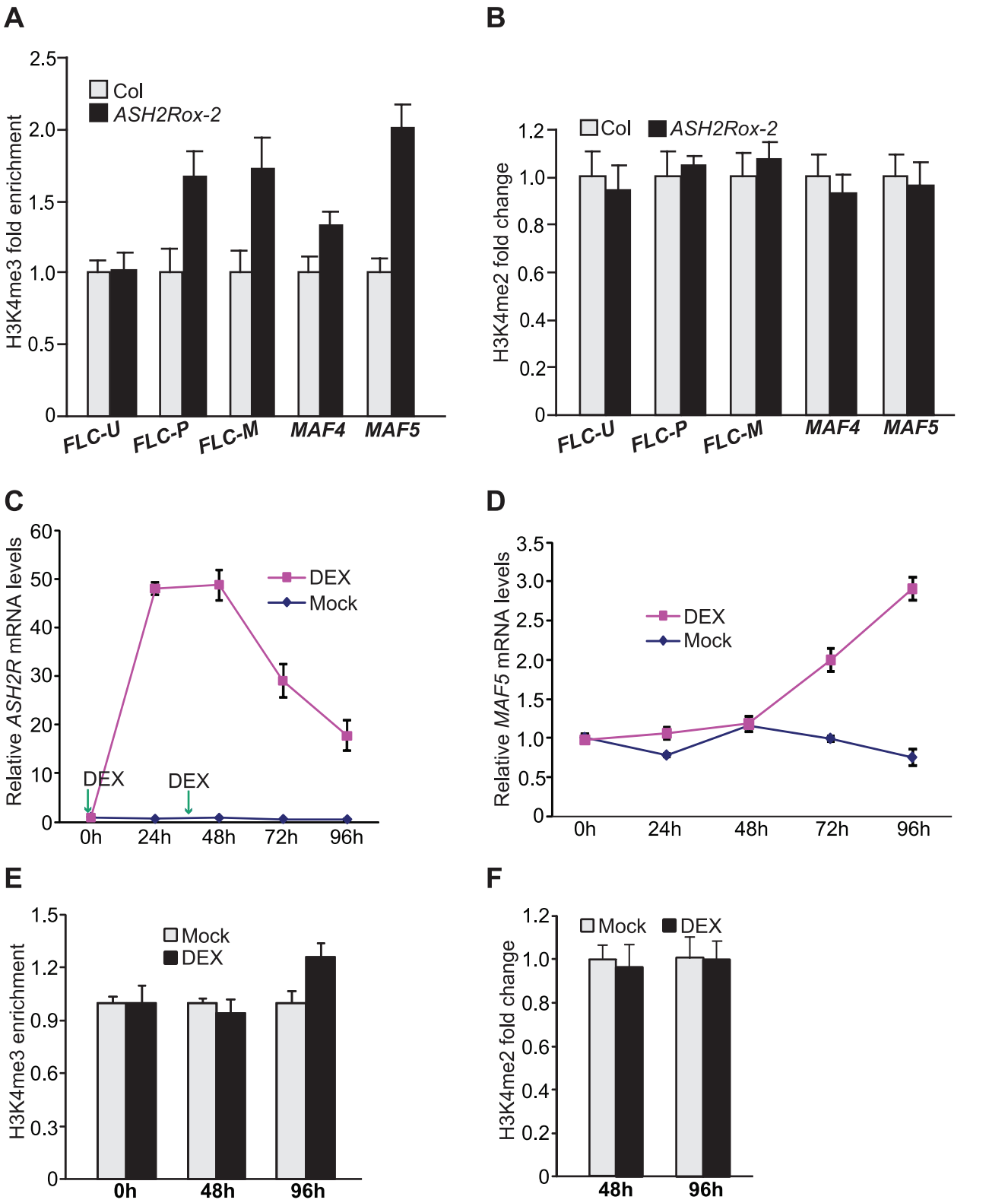

Figure 11. Gain of *ASH2R* Function Leads to Increased H3K4 Trimethylation in Its Direct Target Genes. (A) Analysis of H3K4me3 in *FLC*, *MAF4* and *MAF5* in Col and *ASH2Rox-2* seedlings. The amounts of genomic fragments immunoprecipitated with anti-H3K4me3 were quantified and subsequently normalized to *TUB2*. Relative fold changes of *ASH2Rox-2* over Col at the indicated regions (as illustrated in Figure 10A) are shown. Error bars indicate SD. (B) Relative levels of H3K4me2 in *FLC*, *MAF4* and *MAF5* chromatin in Col and *ASH2Rox-2* seedlings. (C) *ASH2R* expression in the *pOp6-ASH2R;p35S-GR:LhG4* line (in the Col background) upon DEX treatments. Seedlings were treated with 10 μM DEX twice (at 0h and 36h as indicated by the arrows), and shoot apices with newly emerged leaves were harvested 0, 24, 48, 72 and 96 h after the initial treatment. DEX was omitted in the mock control. *ASH2R* transcript levels were quantified by real-time quantitative RT-PCR. Relative expression to 0h is presented; bars indicate SD. Note

that the DEX treatments did not affect *ASH2R* expression in Col. (D) *MAF5* expression in the shoot apices with newly emerged leaves of the *pOp6-ASH2R;p35S-GR:LhG4* line upon DEX treatments as described in (C). Relative expression to 0h is presented; bars indicate SD. Note that the DEX treatments did not affect *MAF5* expression in Col. (E) Analysis of H3K4me3 in *MAF5* chromatin in the shoot apices with newly emerged leaves of the *pOp6-ASH2R;p35S-GR:LhG4* line upon DEX-activated *ASH2R* induction. The DEX treatments were as described in (C). Relative fold changes of DEX-treated over mock samples at the indicated time points are shown. The examined *MAF5* region is as illustrated in Figure 10A. Error bars indicate SD. (F) Analysis of H3K4me2 in *MAF5* chromatin in the shoot apices with newly emerged leaves of the *pOp6-ASH2R;p35S-GR:LhG4* line upon the DEX treatments as described in (C).
doi:10.1371/journal.pgen.1001330.g011

expression and consequent early flowering. Furthermore, we have found that knockdown of either *WDR5a* or *RBL* expression, like *ash2r* and *atx1*, leads to reduced *FLC* expression and early flowering. These genetic findings are consistent with that WDR5a and RBL are part of the ASH2R-ATX1 COMPASS-like complex that activates *FLC* expression.

FLC is expressed at a level relatively low in the Col background (the wild-type accession used in this study and also commonly used in other *Arabidopsis* studies), compared to *FRIGIDA* (*FRI*)-containing accessions (note that *FRI* is mutated in Col) [45]. *FRI*, encoding a coiled-coil domain protein, upregulates the expression of *FLC* to a higher level that significantly delays flowering [45]. Previously, it has been shown that *ATX1* is required for *FRI*-dependent *FLC* upregulation [21]. We have recently revealed that a functional *FRI* causes an increase in the amount of WDR5a protein bound to *FLC* chromatin, resulting in elevated H3K4 trimethylation in *FLC* [24]. *WDR5a* knockdown strongly suppresses *FRI*-dependent *FLC* upregulation, but not *FLC* upregulation/de-repression upon loss of *FLD* function (note that FLD, a putative H3K4 demethylase, represses *FLC* expression) [24]. Similarly, we have observed that *ASH2R* knockdown strongly suppresses *FRI*-dependent *FLC* upregulation, but not *FLC* de-repression in *fld* mutants (data not shown). Given the association of WDR5a with ATX1 and ASH2R (via RBL), these findings suggest that in the presence of a functional *FRI*, the ASH2R-WDR5a-ATX1 COMPASS-like complex is further enriched at *FLC* chromatin to upregulate *FLC* expression. Recently it has been reported that a histone methyltransferase known as EFS, that can methylate both H3K4 and H3K36 *in vitro*, is required for FRI recruitment to the *FLC* locus [46]. This recruitment is expected to cause the enrichment of ASH2R-WDR5a-ATX1 complex at *FLC*, which may function in concert with EFS leading to H3K4 and H3K36 methylation at *FLC* and *FLC* upregulation in the *FRI* background.

We and others have found that a null *ASH2R/TRO* lesion causes arrested embryogenesis at globular stage [see Figure S3 and [38]]; in addition, we found that ASH2R forms the core subcomplex with RBL and WDR5a in developing siliques and is required for genome-wide H3K4 trimethylation. These findings, together with the strong expression of *ASH2R* in developing seeds (Figure 6C, 6D), lead us to conclude that the ASH2R core subcomplex (presumably ASH2R-COMPASS) mediates H3K4 trimethylation in seed chromatin to control seed development. Interestingly, we noticed that knockdown of *RBL* or *WDR5a*, like *ASH2R* knockdown, does not disrupt seed development. There are two possible explanations. Firstly, the dsRNAi targeting *RBL*, *ASH2R* or *WDR5a* driven by the *35S* promoter only partially suppresses target gene expression, and the remaining transcripts may be sufficient for proper embryogenesis. Secondly, *WDR5a*, *ASH2R* or *RBL* expression in the *RNAi* lines may not be affected in early embryogenesis because the *35S* promoter has been shown to be inactive in the early seed development [47].

Role of ASH2R and ASH2R-COMPASS for H3K4 Trimethylation in Higher Plants

In yeast, the intact COMPASS complex is required for di- and tri-methylation of H3K4 [8]. Mammalian Ash2-COMPASS complexes are capable of catalyzing di- and tri-methylation of H3K4 [9,41]; for instance, MLL2 deficiency in mouse oocytes causes a genome-wide reduction in H3K4me2 and H3K4me3 [42]. In mammals, both di- and tri-methylation of H3K4 are associated with actively transcribed genes [5], whereas recent genome-scale studies have revealed that only H3K4me3, but not H3K4me2, is correlated with active transcription and implicated in transcriptional activation in *Arabidopsis* [6]. Because H3K4me3 and H3K4me2 have distinct distribution patterns in *Arabidopsis* genome, they are expected to be deposited by different players. In this study, we have found that loss of *ASH2R* function causes a strong global reduction in H3K4me3, but not in H3K4me2 or H3K4me1 in *Arabidopsis*, whereas *ASH2R* overexpression leads to a genome-wide increase in H3K4me3, but not in H3K4me2 or H3K4me1. Furthermore, we have revealed that *ASH2R* knockdown causes a strong reduction in H3K4me3, but not in H3K4me2, whereas *ASH2R* overexpression leads to an increase in H3K4me3, but not in H3K4me2, in its direct target genes *FLC*, *MAF4* and *MAF5* to activate their expression. These findings further support the notion that the *Arabidopsis* ASH2R-COMPASS complexes specifically deposit H3K4me3 to promote target gene expression, providing a molecular explanation for the observed coupling of H3K4me3 (but not H3K4me2) with active gene expression in *Arabidopsis*. This indicates a difference in the role of Ash2-COMPASS in H3K4 methylation between *Arabidopsis* and yeast/mammals.

Both constitutive overexpression of *ASH2R* and the timed chemical induction of *ASH2R* expression give rise to increased H3K4me3 in its target genes such as *MAF5*, and target gene activation. Interestingly, overexpression of *WDR5a* and *RBL* by the constitutive *35S* promoter, unlike *ASH2R* overexpression, did not give rise to any noticeable phenotypes (data not shown). Together, these observations indicate that the availability of ASH2R protein is a rate-limiting factor in *Arabidopsis* H3K4 trimethylation.

Transcriptional Activation by H3K4 Trimethylation

As noted in Introduction, H3K4 trimethylation is a chromatin mark for actively expressed genes in eukaryotic organisms that so far have been examined, but whether it can activate gene expression has been under much debate [see [16]] as the accumulation of H3K4me3 (predominantly in the 5′ transcribed regions) in actively transcribed chromatin may merely result from active transcription. In this study, we have found that the ASH2R core subcomplex, presumably ASH2R-COMPASS, binds to *FLC*, *MAF4* and *MAF5* chromatin, and that *ASH2R* knockdown leads to a reduction in H3K4me3 and suppresses the expression of these three genes. In addition, *ASH2R* overexpression causes increased H3K4me3 and activation of these gene expression. Furthermore, we have found that timed chemical induction of *ASH2R* expression causes increased H3K4 trimethylation in *MAF5* (a direct target of ASH2R) in shoot apices and turns on its expression. These results strongly suggest that H3K4 trimethylation in *FLC*, *MAF4* and *MAF5* can activate their expression, providing concrete evidence for the notion that H3K4 trimethylation can activate eukaryotic

gene expression. Ash2-COMPASS complexes are expected to be actively recruited to target gene chromatin to catalyze H3K4 trimethylation; subsequently, the evolutionarily conserved ATP-dependent chromatin remodeling factors such as NURF in human that recognizes and binds to H3K4me3 [11], may be recruited to target genes to actively mobilize/remodel nucleosomes, resulting in transcriptional activation or active gene expression.

Materials and Methods

Plant Materials and Growth Conditions

All of the *Arabidopsis thaliana* lines used in this study were in the Col background. The *ash2r-1* allele (SAIL_851_H01) was isolated from the SAIL collection [39]. Plants were grown under cool white fluorescent lights in long days (16h light/8h dark).

Yeast Two-Hybrid Assay

The Matchmaker GAL4 Two-Hybrid System 3 (Clontech) was adapted for the yeast two-hybrid assay. The full-length coding sequences for the tested genes were cloned into the *pGADT7* and/or *pGBKT7* vectors (Clontech). The experiments were performed according to the manufacturer's instructions using the strain *AH109* (Clontech). To test the interactions, yeast cells were spotted on the highly selective SD media lacking of leucine, tryptophan, histidine and adenine.

Bimolecular Fluorescence Complementation Analysis

The full-length coding sequences for *WDR5a*, *ASH2R*, *RBL*, *SDG14* and *SDG16* were translationally fused with either an N-terminal *EYFP* fragment in the *pSAT1A-nEYFP-N1/pSAT1-nEYFP-C1* vectors and/or a C-terminal *EYFP* fragment in the *pSAT1A-cEYFP-N1/pSAT1-cEYFP-C1-B* vectors (www.bio.purdue.edu/people/faculty/gelvin/nsf/index.htm). Onion epidermal cells were transiently co-transformed by appropriate plasmid pairs using the Helium biolistic gene transformation system (Bio-Rad) following the manufacturer's instructions. Within 24–48 hrs after bombardment, YFP fluorescence was observed and imaged using a Zeiss LSM 5 EXCITER upright laser scanning confocal microscopy (Zeiss).

Whole-Mounted Clearing of Seeds

For the examination of seed development, seeds were cleared in 8:1:3 (W/V/V) chloral hydrate:glycerol: water for 1–2 hrs. The cleared seeds were examined using differential-interference-contrast optics on a Leica DM4500B microscope, and images were acquired with a Nikon DXM1200F digital camera.

Plasmid Constructions

To knock down *RBL* expression, two copies of a 245-bp *RBL* specific fragment (from +1853 to +2097 of the *RBL* cDNA; TSS as +1) were inserted into the *pB7GWIWG2* vector [48] for hairpin RNA production. For *ASH2R* knockdown, two copies of a 223-bp *ASH2R*-specific fragment (from +1456 to +1678 of the *ASH2* cDNA; TSS as +1), were inserted into the *pB7GWIWG2* vector for hairpin RNA production. For overexpression of *ASH2R* and the rescue of *ash2r-1* mutant, the full-length coding sequence for *ASH2R* was inserted downstream of the CaMV *35S* promoter in the *pMDC32* vector [49] via gateway technology (Invitrogen), resulting in the *35S-ASH2R* construct. For *ASH2R:FLAG* construction, the full-length *ASH2R* coding sequence except the stop codon was first fused in frame with a *FLAG* tag (three copies), and subsequently the *ASH2R-FLAG* fragment was inserted downstream of the *35S* promoter in the *pMDC32* vector via gateway technology.

For ASH2R subcellular localization, the full-length *ASH2R* coding sequence except the stop codon was inserted between the *35S* promoter and *GFP* in the *pMDC85* vector [49]; the *ASH2R* coding sequence was in frame with the downstream *GFP* reporter gene. For *ASH2R-GUS* construction, an 1816-bp *ASH2R* genomic fragment (from −1537 to +279; A of the start codon as +1) including a 1537-bp native promoter and a 279-bp genomic coding region was inserted upstream of the *GUS* reporter gene in the *pMDC162* vector [49]; the genomic coding sequence was in frame with *GUS*. To construct *RBL-GUS*, we inserted a 1665-bp *RBL* genomic fragment (from −1081 to +584; A of the start codon as +1) upstream of the *GUS* reporter gene in *pMDC162*; the genomic coding sequence of *RBL* was in frame with *GUS*.

Real-Time Quantitative RT-PCR

Total RNAs were extracted from aerial parts of 10-d-old seedlings or DEX-treated tissues as described previously [50]. The total RNAs were subsequently used as templates to synthesize cDNAs by reverse transcription. Real-time quantitative PCR was carried out on an ABI Prism 7900HT sequence detection system as previously described [24,50]. Primers used to amplify the cDNAs of *FLC*, *FLM*, *MAF2-MAF5* and *TUB2* (At_*5g62690*) have been previously described [29,50]. The primer pair, 5′-AGGAAGGGTACAAGGAAGGTGATG-3′ and 5′-AACGATATTTCACTGCCTGGTACAAC-3′, was used for *ASH2R* amplification; the primer pair, 5′-CGAAGATGAATTTGATTTGATACCTG-3′ and 5′-TGTCTCACCCATTTCTTCTGCTTGT-3′, was used to amplify *RBL* cDNAs. Each sample was quantified in triplicate and normalized to the endogenous control *TUB2*. Bars indicate standard deviations of triplicate measurements.

Histochemical β-Glucuronidase Staining

Plant tissues were fixed in 80% acetone at −20°C for 1 hr, washed by a staining buffer (5 mM EDTA pH 8.0, 0.05% Triton X-100, 2 mM potassium ferrocyanide, 2 mM potassium ferricyanide, 100 mM NaH_2PO4 and 100 mM Na_2HPO4), and incubated in the staining buffer with 0.5-mg 5-bromo-4-chloro-3-indolyl-β-d-glucuronic acid (X-Gluc) at 37°C for 4 to 12 hrs. The *ASH2R-GUS* seedlings were stained for 4 hrs, and other stainings were performed for 12 hrs. Seeds were cleared after staining for observation under a Leica DM4500B microscope.

Co-Immunoprecipitation

Immunoprecipitation experiments were performed as described previously [51] with minor modifications. Briefly, about 0.5-g 10-d-old seedlings were harvested and ground in liquid nitrogen, and subsequently, total proteins were extracted. 1.0-ml protein extracts were incubated with 60-µl slurry of anti-FLAG M2 affinity gel (Sigma, Cat#: A2220), and the immunoprecipitated proteins were washed three times and subsequently boiled in the SDS-PAGE loading buffer, followed by western blotting with anti-FLAG (Sigma, Cat#: A8592) or anti-WDR5 [Abcam, Cat#: ab75439 (Batch #: 639695); note that this antibody recognizes WDR5a; see [24]]. In the immunoprecipitation experiments with 5-DAP siliques, the samples were cross-linked with 1% formaldehyde for 30 minute before protein extraction as described previously [51].

Histone Extraction and Immunoblotting

Histone protein extraction and western analysis were performed as previously described [29]. Briefly, total histones were extracted from 10-d-old seedlings, separated in an SDS-PAGE gel, and transferred to a 0.2-µl nitrocellulose membrane (Bio-Rad). The protein blots were probed with anti-monomethyl histone H3K4

(Abcam, Cat#: ab8895), anti-dimethyl H3K4 (Millipore, Cat#: 07-030), anti-trimethyl H3K4 (Millipore, Cat#: 05-745R) and anti-histone H3 (Millipore, Cat#: 07-690).

ChIP-Quantitative PCR

ChIP experiments were performed with 10-d-old seedlings or DEX-treated shoot apices including newly emerged leaves as previously described [52]. Immunoprecipitations were carried out using Rabbit polyclonal anti-dimethyl H3K4 (Millipore, Cat#: 07-030), anti-trimethyl H3K4 (Millipore, Cat#: 05-745R) or anti-FLAG (Sigma, Cat#: A8592). The real-time quantitative PCR and the primers used to amplify *FLC-U*, *FLC-P*, *FLC-M* and *TUB2* were described previously [29,50]. The primer pair, 5′-CGGCGAGTTATGCAGACATCACA-3′ and 5′-GTGGCAGAGATGATGATAAGAGCG A-3′, was used to amplify *MAF4*; the primer pair, 5′-CAGGATCTCCGACCAGTTTATACAGAC-3′ and 5′-GAGGAGTTGTAGAGTTTGCCGGT-3′, was used to amplify *MAF5*. The *MAF3* region was amplified by the primer pair: 5′-GTCTAGCCCAAAAGAAGAAGATAGAAACG-3′ and 5′-GGAGGCAGAGTCGTAGAGTTTTCC-3′. The relative fold changes are the averages of two independent biological repeats.

DEX Treatments

The initial treatments were carried out by applying 10 μM DEX plus 0.015% Silwet L-77 to 7-d old seedlings of Col and the *pOp6-ASH2R;p35S-GR:LhG4* line grown in long days (the second treatment was carried out 36h after the initial treatment). In the mock control, DEX was omitted. The hour of initial DEX application was designated as 0h. Shoot apices including newly emerged leaves or the first pair of rosette leaves were collected at 0, 24, 48, 72 and 96h for RNA analyses. For ChIP experiments, shoot apices with newly emerged leaves were collected at 0, 48 and 96h.

Supporting Information

Figure S1 Alignment of *Arabidopsis* ASH2R (At ASH2R) with *Homo sapiens* Ash2 (Hs Ash2) and *S. cerevisiae* BRE2 (Sc BRE2). Numbers refer to amino acid residues. Identical residues among these proteins are shaded black, whereas similar residues are shaded gray.
Found at: doi:10.1371/journal.pgen.1001330.s001 (1.53 MB TIF)

Figure S2 Analysis of the Human RbBP5 Homologs in Representative Animal and Plant Species. (A) Alignment of *Arabidopsis* RBL (At RBL) with *Homo sapiens* RbBP5 (Hs RbBP5) and *S. cerevisiae* SWD1 (Sc SWD1). Numbers refer to amino acid residues. Identical residues among these proteins are shaded black, whereas similar residues are shaded gray. (B) Phylogenetic tree analysis of RbBP5 homologs from representative plant and animal species. The tree of full-length RbBP5 homologs was constructed by the Neighbor-Joining method using PHYLIP. Bootstrap values are shown for clades with support greater than 60% (in 1000 sampling replicates). The protein accession numbers are specified in Table S1.
Found at: doi:10.1371/journal.pgen.1001330.s002 (1.83 MB TIF)

Figure S3 *ASH2R* Is Essential for Embryo and Seed Development. (A) Wildtype (Col) and *ash2r-1*/+ heterozygote siliques. Portions of siliques were shown; arrows indicate aborted white and brown seeds. Shown on the right is an *ash2r-1* (null) silique carrying the *p35S-ASH2R* transgene made of *ASH2R CDS* driven by the *35S* promoter. (B–E) Wild-type seeds with globular embryo (B), with procambial embryo (C), with triangular embryo (D), and with heart embryo (E). (F, G and H) are *ash2r-1* mutant seeds (with globular embryo) from the *ash2r-1*/+ siliques in which embryos with a wild-type phenotype were at procambial, triangular and heart stages, respectively. (B to H) Scale bars are 50 μm.
Found at: doi:10.1371/journal.pgen.1001330.s003 (4.09 MB TIF)

Figure S4 Analysis of the Point-Mutated *ASH2R* Transgene. (A) Schematic structure of the *ASH2R* transgene construct. Arrows indicate translation start sites. *pOp6* is a synthetic promoter consists of six copies of the *lac* operator and the *35S* minimal promoter. *GR:LhG4* driven by the *35S* promoter encodes a transcriptional activator whose active form can bind to *pOp6*. (B) Alignment of *Arabidopsis* ASH2R (At ASH2R) with *Populus trichocarpa* ASH2R (Pt ASH2R), *Ricinus communis* ASH2R (Rc ASH2R) and *Vitis vinifera* ASH2R (Vv ASH2R). Two missense point mutations introduced into the *ASH2R* transgene are indicated with stars. Numbers refer to amino acid residues. Identical residues among these proteins are shaded black, whereas similar residues are shaded gray.
Found at: doi:10.1371/journal.pgen.1001330.s004 (3.02 MB TIF)

Figure S5 Percentage of Seed-Bearing Siliques of Col, *ash2r-2^{hyp}*, and *ash2r-3^{hyp}*. Forty, sixty-six and eight-nine siliques or silique-like structures from main shoots were examined for Col, *ash2r-2^{hyp}* and *ash2r-3^{hyp}*, respectively.
Found at: doi:10.1371/journal.pgen.1001330.s005 (0.51 MB EPS)

Figure S6 Relative *ASH2R* mRNA Levels in the *ASH2Rox* Seedlings Determined by Real-Time Quantitative PCR. Relative expression to parental Col is presented. Bars indicate SD.
Found at: doi:10.1371/journal.pgen.1001330.s006 (0.50 MB EPS)

Figure S7 WDR5b Does Not Interact with RBL or ASH2R. Full-length WDR5b and the indicated proteins were fused with the GAL4-BD or AD domain. Yeast cells harboring these fusions, AD and/or BD, as indicated, were grown on SD media lacking Trp and Leu and selective SD media lacking of Trp, Leu, His and adenine. Note that AD-WDR5b was expressed in yeast as it could interact with an *Arabidopsis* protein in an unrelated yeast two-hybrid assay.
Found at: doi:10.1371/journal.pgen.1001330.s007 (8.00 MB TIF)

Figure S8 ASH2R Protein Subcellular Localization. The ASH2R-GFP fusion protein is localized in nuclei as indicated by the green fluorescence signals in *Arabidopsis* roots. Blue DAPI staining indicates nuclei.
Found at: doi:10.1371/journal.pgen.1001330.s008 (2.06 MB EPS)

Figure S9 RBL or ASH2R Does Not Interact with Putative H3K4 Methyltransferases. Yeast cells harboring the indicated fusions were grown on SD media lacking Trp and Leu, and selective SD media lacking of Trp, Leu, His and adenine.
Found at: doi:10.1371/journal.pgen.1001330.s009 (9.30 MB TIF)

Figure S10 Timed Activation of *ASH2R* Expression by DEX and Subsequent *MAF5* Induction. (A) Schematic structure of the *pOp6-ASH2R;p35S-GR:LhG4* construct. Arrows indicate translation start sites. (B) *ASH2R* expression in the *pOp6-ASH2R;p35S-GR:LhG4* line upon DEX treatment. 7-d-old seedlings were treated with 10 μM DEX once (at 0h), and shoot apices with newly emerged leaves were harvested 0, 24, 48, 72 and 96 h after the DEX application. DEX was omitted in the mock control. *ASH2R* transcript levels were quantified by real-time quantitative RT-PCR. Relative expression to 0 h is presented; bars indicate SD. (C) *MAF5* expression in the shoot apices with newly emerged leaves of the *pOp6-ASH2R;p35S-GR:LhG4* line upon DEX treatment. The treatment was as described in (C). Relative expression to 0 h is presented; bars indicate SD. (D) *ASH2R* expression in the first pair of rosette leaves of the *pOp6-ASH2R;p35S-GR:LhG4* line upon

DEX treatment. Seedlings were treated with 10 μM DEX twice (at 0 h and 36 h), and rosette leaves were harvested 0, 24, 48, 72 and 96 h after the initial treatment. Relative expression to 0 h is presented; bars indicate SD. (E) *MAF5* expression in the first pair of rosette leaves of the *pOp6-ASH2R;p35S-GR:LhG4* line upon DEX treatment. The treatment was as described in (D). Relative expression to 0 h is presented; bars indicate SD.
Found at: doi:10.1371/journal.pgen.1001330.s010 (1.23 MB EPS)

Table S1 List of WDR5 and RbBP5 Homologs from Representative Animal and Plant Species.
Found at: doi:10.1371/journal.pgen.1001330.s011 (0.04 MB DOC)

Acknowledgments

We thank Toshiro Ito for critically reading this manuscript, Stan Gevin for generously providing the BiFC vectors, and Flanders Interuniversity Institute for Biotechnology (Belgium) for providing the *pB7GWIWG2* vector.

Author Contributions

Conceived and designed the experiments: DJ NCK XG YH. Performed the experiments: DJ NCK XG ZL. Analyzed the data: DJ NCK XG ZL YH. Wrote the paper: YH.

References

1. Lan F, Nottke AC, Shi Y (2008) Mechanisms involved in the regulation of histone lysine demethylases. Curr Opin Cell Biol 20: 316–325.
2. Shilatifard A (2008) Molecular implementation and physiological roles for histone H3 lysine 4 (H3K4) methylation. Curr Opin Cell Biol 20: 341–348.
3. Santos-Rosa H, Schneider R, Bannister AJ, Sherriff J, Bernstein BE, et al. (2002) Active genes are tri-methylated at K4 of histone H3. Nature 419: 407–411.
4. Schubeler D, MacAlpine DM, Scalzo D, Wirbelauer C, Kooperberg C, et al. (2004) The histone modification pattern of active genes revealed through genome-wide chromatin analysis of a higher eukaryote. Genes Dev 18: 1263–1271.
5. Bernstein BE, Kamal M, Lindblad-Toh K, Bekiranov S, Bailey DK, et al. (2005) Genomic maps and comparative analysis of histone modifications in human and mouse. Cell 120: 169–181.
6. Zhang X, Bernatavichute YV, Cokus S, Pellegrini M, Jacobsen SE (2009) Genome-wide analysis of mono-, di- and trimethylation of histone H3 lysine 4 in *Arabidopsis thaliana*. Genome Biol 10: R62.
7. Miller T, Krogan NJ, Dover J, Erdjument-Bromage H, Tempst P, et al. (2001) COMPASS: a complex of proteins associated with a trithorax-related SET domain protein. Proc Natl Acad Sci U S A 98: 12902–12907.
8. Schneider J, Wood A, Lee JS, Schuster R, Dueker J, et al. (2005) Molecular regulation of histone H3 trimethylation by COMPASS and the regulation of gene expression. Mol Cell 19: 849–856.
9. Dou Y, Milne TA, Ruthenburg AJ, Lee S, Lee JW, et al. (2006) Regulation of MLL1 H3K4 methyltransferase activity by its core components. Nat Struct Mol Biol 13: 713–719.
10. Ruthenburg AJ, Allis CD, Wysocka J (2007) Methylation of lysine 4 on histone H3: intricacy of writing and reading a single epigenetic mark. Mol Cell 25: 15–30.
11. Sims RJ, Reinberg D (2006) Histone H3 Lys 4 methylation: caught in a bind? Genes Dev 20: 2779–2786.
12. Ng HH, Robert F, Young RA, Struhl K (2003) Targeted recruitment of Set1 histone methylase by elongating Pol II provides a localized mark and memory of recent transcriptional activity. Mol Cell 11: 709–719.
13. He Y, Doyle MR, Amasino RM (2004) PAF1-complex-mediated histone methylation of *FLOWERING LOCUS C* chromatin is required for the vernalization-responsive, winter-annual habit in *Arabidopsis*. Genes Dev 18: 2774–2784.
14. Zhu B, Mandal SS, Pham AD, Zheng Y, Erdjument-Bromage H, et al. (2005) The human PAF complex coordinates transcription with events downstream of RNA synthesis. Genes Dev 19: 1668–1673.
15. Oh S, Park S, van Nocker S (2008) Genic and global functions for Paf1c in chromatin modification and gene expression in *Arabidopsis*. PLoS Genet 4: e1000077. doi:10.1371/journal.pgen.1000077.
16. Henikoff S (2008) Nucleosome destabilization in the epigenetic regulation of gene expression. Nat Rev Genet 9: 15–26.
17. Springer NM, Napoli CA, Selinger DA, Pandey R, Cone KC, et al. (2003) Comparative analysis of SET domain proteins in *maize* and *Arabidopsis* reveals multiple duplications preceding the divergence of monocots and dicots. Plant Physiol 132: 907–925.
18. Baumbusch LO, Thorstensen T, Krauss V, Fischer A, Naumann K, et al. (2001) The *Arabidopsis thaliana* genome contains at least 29 active genes encoding SET domain proteins that can be assigned to four evolutionarily conserved classes. Nucleic Acids Res 29: 4319–4333.
19. Alvarez-Venegas R, Avramova Z (2005) Methylation patterns of histone H3 Lys 4, Lys 9 and Lys 27 in transcriptionally active and inactive *Arabidopsis* genes and in *atx1* mutants. Nucleic Acids Res 33: 5199–5207.
20. Alvarez-Venegas R, Pien S, Sadder M, Witmer X, Grossniklaus U, et al. (2003) *ATX-1*, an *Arabidopsis* homolog of *TRITHORAX*, activates flower homeotic genes. Curr Biol 13: 627–637.
21. Pien S, Fleury D, Mylne JS, Crevillen P, Inze D, et al. (2008) *ARABIDOPSIS TRITHORAX1* dynamically regulates *FLOWERING LOCUS C* activation via histone H3 lysine-4 trimethylation. Plant Cell 20: 580–588.
22. Tamada Y, Yun JY, Woo SC, Amasino RM (2009) *ARABIDOPSIS TRITHORAX-RELATED7* is required for methylation of lysine 4 of histone H3 and for transcriptional activation of *FLOWERING LOCUS C*. Plant Cell 21: 3257–3269.
23. Berr A, Xu L, Gao J, Cognat V, Steinmetz A, et al. (2009) *SET DOMAIN GROUP25* encodes a histone methyltransferase and is involved in *FLOWERING LOCUS C* activation and repression of flowering. Plant Physiol 151: 1476–1485.
24. Jiang D, Gu X, He Y (2009) Establishment of the winter-annual growth habit via FRIGIDA-mediated histone methylation at *FLOWERING LOCUS C* in *Arabidopsis*. Plant Cell 21: 1733–1746.
25. Michaels SD (2009) Flowering time regulation produces much fruit. Curr Opin Plant Biol 12: 75–80.
26. Baurle I, Dean C (2006) The timing of developmental transitions in plants. Cell 125: 655–664.
27. Scortecci KC, Michaels SD, Amasino RM (2001) Identification of a MADS-box gene, *FLOWERING LOCUS M*, that represses flowering. Plant J 26: 229–236.
28. Ratcliffe OJ, Kumimoto RW, Wong BJ, Riechmann JL (2003) Analysis of the *Arabidopsis MADS AFFECTING FLOWERING* gene family: *MAF2* prevents vernalization by short periods of cold. Plant Cell 15: 1159–1169.
29. Gu X, Jiang D, Wang Y, Bachmair A, He Y (2009) Repression of the floral transition via histone H2B monoubiquitination. Plant J 57: 522–533.
30. Sung S, Amasino RM (2005) REMEMBERING WINTER: Toward a molecular understanding of vernalization. Annu Rev Plant Biol 56: 491–508.
31. He Y (2009) Control of the transition to flowering by chromatin modifications. Molecular Plant 2: 554–564.
32. Schubert D, Primavesi L, Bishopp A, Roberts G, Doonan J, et al. (2006) Silencing by plant Polycomb-group genes requires dispersed trimethylation of histone H3 at lysine 27. Embo J 25: 4638–4649.
33. Wu K, Zhang L, Zhou C, Yu CW, Chaikam V (2008) *HDA6* is required for jasmonate response, senescence and flowering in *Arabidopsis*. J Exp Bot 59: 225–234.
34. Schmitz RJ, Sung S, Amasino RM (2008) Histone arginine methylation is required for vernalization-induced epigenetic silencing of *FLC* in winter-annual *Arabidopsis thaliana*. Proc Natl Acad Sci U S A 105: 411–416.
35. Wang X, Zhang Y, Ma Q, Zhang Z, Xue Y, et al. (2007) SKB1-mediated symmetric dimethylation of histone H4R3 controls flowering time in *Arabidopsis*. Embo J 26: 1934–1941.
36. Liu C, Lu F, Cui X, Cao X (2010) Histone methylation in higher plants. Annu Rev Plant Biol 61: 395–420.
37. Yu X, Michaels SD (2010) The *Arabidopsis* Paf1c complex component CDC73 participates in the modification of *FLC* chromatin. Plant Physiol: 153: 1074–1084.
38. Aquea F, Johnston AJ, Canon P, Grossniklaus U, Arce-Johnson P (2010) *TRAUCO*, a *Trithorax*-group gene homologue, is required for early embryogenesis in *Arabidopsis thaliana*. J Exp Bot 61: 1215–1224.
39. Sessions A, Burke E, Presting G, Aux G, McElver J, et al. (2002) A high-throughput *Arabidopsis* reverse genetics system. Plant Cell 14: 2985–2994.
40. Craft J, Samalova M, Baroux C, Townley H, Martinez A, et al. (2005) New *pOp/LhG4* vectors for stringent glucocorticoid-dependent transgene expression in *Arabidopsis*. Plant J 41: 899–918.
41. Patel A, Vought VE, Dharmarajan V, Cosgrove MS (2008) A conserved arginine-containing motif crucial for the assembly and enzymatic activity of the Mixed Lineage Leukemia Protein-1 core complex. J Biol Chem 283: 32162–32175.
42. Andreu-Vieyra CV, Chen R, Agno JE, Glaser S, Anastassiadis K, et al. (2010) MLL2 is required in oocytes for bulk Histone 3 lysine 4 trimethylation and transcriptional silencing. PLoS Biol 8: e1000453. doi:10.1371/journal.pbio.1000453.
43. Sun B, Xu Y, Ng KH, Ito T (2009) A timing mechanism for stem cell maintenance and differentiation in the *Arabidopsis* floral meristem. Genes Dev 23: 1791–1804.
44. Reddy GV, Meyerowitz EM (2005) Stem-cell homeostasis and growth dynamics can be uncoupled in the *Arabidopsis* shoot apex. Science 310: 663–667.
45. Johanson U, West J, Lister C, Michaels S, Amasino R, et al. (2000) Molecular analysis of *FRIGIDA*, a major determinant of natural variation in *Arabidopsis* flowering time. Science 290: 344–347.

46. Ko JH, Mitina I, Tamada Y, Hyun Y, Choi Y, et al. Growth habit determination by the balance of histone methylation activities in *Arabidopsis*. Embo J 29: 3208–3215.
47. Kwong RW, Bui AQ, Lee H, Kwong LW, Fischer RL, et al. (2003) *LEAFY COTYLEDON1-LIKE* defines a class of regulators essential for embryo development. Plant Cell 15: 5–18.
48. Karimi M, De Meyer B, Hilson P (2005) Modular cloning in plant cells. Trends Plant Sci 10: 103–105.
49. Curtis MD, Grossniklaus U (2003) A gateway cloning vector set for high-throughput functional analysis of genes *in planta*. Plant Physiol 133: 462–469.
50. Jiang D, Yang W, He Y, Amasino RM (2007) *Arabidopsis* relatives of the human Lysine-Specific Demethylase1 repress the expression of *FWA* and *FLOWERING LOCUS C* and thus promote the floral transition. Plant Cell 19: 2975–2987.
51. Wood CC, Robertson M, Tanner G, Peacock WJ, Dennis ES, et al. (2006) The *Arabidopsis thaliana* vernalization response requires a Polycomb-like protein complex that also includes VERNALIZATION INSENSITIVE 3. Proc Natl Acad Sci U S A 103: 14631–14636.
52. Johnson L, Cao X, Jacobsen S (2002) Interplay between two epigenetic marks: DNA methylation and histone H3 lysine 9 methylation. Curr Biol 12: 1360–1367.